Received 1 November 2024; revised 6 December 2024; accepted 19 December 2024. Date of publication 23 December 2024; date of current version 8 January 2025.

Digital Object Identifier 10.1109/OJCOMS.2024.3521503

A Generic Millimeter Wave and Terahertz Spectrum Reuse Model for In-Building Multi-Band Small Cells: Achieving Spectral and Energy Efficiencies of 6G

RONY K. SAHA [1,2]

[1] Department of Electrical and Electronic Engineering, BSRM School of Engineering, BRAC University, Dhaka 1212, Bangladesh
[2] Dynamic Spectrum Management Group, Department of Electrical Engineering, Stanford University, Stanford, CA 94305, USA

CORRESPONDING AUTHOR: R. K. SAHA (e-mail: rony.saha@bracu.ac.bd)

This work was supported by the BSRM School of Engineering Research Endowment Fund at BRAC University, Dhaka, Bangladesh.

ABSTRACT This paper presents a generic spectrum reuse model (GSRM) to reuse millimeter wave (mmWave) and terahertz (THz) spectrum in multi-band-enabled small cells located within multi-story buildings to address high spectral and energy efficiencies of sixth-generation (6G) mobile networks. For mmWave and THz bands, we consider 28 GHz, 142 GHz, 250 GHz, and 300 GHz bands, and each small cell is assumed to be equipped with these multiple bands. In developing GSRM, we first characterize interferences to derive a minimum distance between apartments of co-channel small cells at both intra-floor and inter-floor levels for each band leading to the formation of a 3-dimensional (3D) cluster of apartments such that the whole spectrum of the corresponding band is allocated to small cells within the cluster. The same spectrum is reused further in small cells of all adjacent 3D clusters within the building. We consider a random distribution of small cells within each 3D cluster. Two scenarios are considered where scenario 1 has the same 3D cluster size for each band, and scenario 2 considers different 3D cluster sizes corresponding to the respective band. We formulate the spectral efficiency (SE) and energy efficiency (EE) metrics of the proposed GSRM in a multi-tier network and develop an algorithm to evaluate its SE and EE metrics. With extensive system-wide evaluations, we show that compared to scenario 1, the overall SE and EE in scenario 2 are improved by 33.33% and 4.5%, respectively, and the proposed GSRM can achieve the prospective SE and EE requirements for 6G mobile systems.

INDEX TERMS 6G, small cell, in-building, spectral efficiency, energy efficiency, spectrum reuse, mobile network, millimeter wave, terahertz, multi-band.

I. INTRODUCTION

In this section, we first give a brief overview of the evolution of spectrum usage toward high-frequency bands with ever-increasing high capacity and data rate demand in mobile networks. As most mobile data is generated indoors, we discuss pertinent characteristics and limitations of the high-frequency spectrum, particularly millimeter wave (mmWave) and terahertz (THz), to reuse them in indoor environments to set relevant background for the reader at the beginning of the paper. Related works on indoor spectrum reuse carried out in the existing literature are surveyed to find potential research gaps and present effective contributions to address them, leading to achieving target performance gains.

A. BACKGROUND ON MMWAVE AND THZ SPECTRUM

In the World Radiocommunication Conference (WRC) 2015, depending on several factors, including channel propagation and global agreement, the International Telecommunication Union (ITU) selected a list of proposed frequencies in the range between 24 GHz and 86 GHz for the global usage [1] of which 28 GHz for the mobile communication and 70 GHz, 80 GHz, and 90 GHz for the ultra-dense network scenario. In WRC 2019, a 17.25 GHz spectrum in total was identified for the mmWave band [2], while a spectrum in total of 160 GHz was identified in the THz ranging from 252 GHz to 450 GHz of which from 306 GHz to 450 GHz was identified as suitable for short-range indoor communications.

The spectrum bandwidth in conventional microwave bands is insufficient to address the growing demands for high capacity and user data rates. This causes us to seek the availability of new spectrum in higher bands, including mmWave and THz bands. However, signal propagations at mmWave and THz bands differ considerably from those at microwave bands. Particularly, because the propagation characteristics of the line-of-sight (LOS) links are superior to that of the non-line-of-sight (NLOS), mmWave communications rely significantly on the presence of LOS links [3]. Further, mmWave signals face severe path loss and are more vulnerable to blockages and penetration losses. For instance, mmWave signals face severe difficulty penetrating through barriers such as furniture, doors, and walls. When propagating through, it was found that a considerable amount of penetration losses of 24.4 decibels (dB) for two walls and 45.1 dB for four doors [4] were faced by 28 GHz mmWave signals. Likewise, mmWave signals can experience from 20 dB to 40 dB due to a single obstruction. The reflection loss due to building materials like bricks is around 40 dB-80 dB, a glass of 3 dB-18 dB, and the foliage loss of a single tree of 17 dB-25 dB [5], [6], [7], [8]. Also, an attenuation of around 20 dB to 35 dB can be caused by the human body [7]. All these blockages eventually degrade the signal strength considerably, leading to a total outage.

Besides, signal blockages and penetration losses cause the transmission of mmWave signal highly directional. The high directivity of mmWave, however, helps mitigate interference, which in turn facilitates dense deployment of small cells in indoor environments to address high capacity and data rate demands of fifth-generation (5G) and beyond mobile networks by reusing mmWave spectrum more in small cells [9], [10], [11] than the microwave frequency. Because the user plane services are typically higher than that of the control plane, a mmWave system may need to coexist with the conventional sub-6 GHz microwave system so that the microwave system can serve all sorts of control plane services, while the mmWave system can serve user plane services. This coexistence of the microwave and mmWave spectrum in turn results in higher capacity and better throughput than that when serving both control and data planes' services with either the microwave or the mmWave spectrum [12].

The frequency of THz signals is higher than that of the mmWave signals causing it to face almost all the challenges that mmWave signals experience as discussed above. Because of smaller coverage than that of mmWave signals, the communication at the THz band is even more limited and difficult when compared with mmWave bands. In fact, a coverage of about 10 meters can be provided using the THz band [13]. However, because of the small coverage of THz bands, the same THz frequency can be reused for indoor small cells [14]. Likewise, because of the small coverage and high directivity, THz signals allow sharing more spectrum efficiently with minimal coordination.

Hence, though both mmWave and THz bands can serve high data rate and capacity requirements of 5G and beyond networks, some emerging applications, including 3-dimensional (3D) gaming and extended reality, may not be possible to be served by mmWave signals. This is because such applications require very high data rates, from several hundred Gigabits per second to several terabits per second. Moreover, the contiguous available spectrum in the mmWave frequency is less than 10 GHz. This has caused the researchers to explore the THz spectrum with an available bandwidth of a few tens of GHz that is capable of supporting a data rate in the range of terabits per second in the sixth-generation (6G) and beyond mobile systems. In short, given the high potentiality of THz bands, particularly, in the indoor, THz bands are considered to be the promising research direction that can complement the sub-6 GHz and mmWave bands to address high data rates and capacity requirements of 6G and beyond systems [15], [16].

B. RELATED WORK

The demand for ever-increasing high capacity and data rate in mobile wireless communications has steadily risen, particularly in indoor environments. In line with this, though the latest mobile generation (i.e., 5G) is in operation, several existing mobile operators still operate their networks on 2G, 3G, and 4G LTE systems [17]. This requires designing base stations equipped with multiple bands to support multiple generations of mobile technologies [18] to enhance network capacity by operating base stations on multifrequency bands. Several studies have already addressed the design of multi-band base stations. For example, authors in [19] proposed a dual-broadband multiple-input multiple-output (MIMO) indoor base station antenna that operates at 800-960 MHz and 1700-2700 MHz simultaneously for second-generation (2G), third-generation (3G), and long-term evolution (LTE) systems. Likewise, in [20], the authors proposed a new design of a triple-band dual-polarized indoor base station antenna to serve 2G, 3G, fourth-generation (4G), and the new sub-6 GHz 5G applications.

Moreover, several works addressed designing multi-band operations in 5G sub-6 GHz bands. For example, authors in [18], presented and evaluated a dual-band high-gain beam steering antenna array for a 5G sub-6 GHz base station operating at 2.2 GHz and 3.8 GHz bands. In [21], authors designed a dual-band MIMO antenna system for sub-6 GHz 5G wireless applications to operate in the 3.3-3.8 GHz and 4.8-5.0 GHz frequency bands. Likewise, numerous studies considered multi-band operations in 5G mmWave bands. For example, authors in [22] proposed a dual-band and dual-polarized antenna-in-package design for 5G user equipment (UE) applications in the 28 and 38 GHz bands. Likewise, in [23], a novel compact dual-band MIMO antenna is suggested for use in 5G mmWave wireless communication applications operating at 28 GHz and 48 GHz bands.

Apart from the same mobile system, multi-band base stations can also share the spectrum of a different system operating at either a licensed band or an unlicensed band. Numerous studies have already been carried out in this regard. For example, authors in [24] examined the multi-band-enabled indoor base stations each operating at both the satellite and terrestrial-mobile spectrums. Further, in [25], authors presented a coexistence mechanism for 5G New Radio on Unlicensed (NR-U) to coexist with Wireless Gigabit (WiGig) by enabling each small cell with dual bands operating at the 60 GHz unlicensed and 28 GHz licensed mmWave bands. Other effective techniques to boost the network capacity are spectrum sharing, spectrum trading, and spectrum segmentation. Each technique however comes with relative pros and cons.

One of the important facts in indoor multi-storage buildings is that, at a high frequency, the coverage area of a small cell base station (SCBS) is limited due to diverse propagation and channel characteristics compared to that outdoors. These inherent signal characteristics at high frequencies allow us to explore SCBSs by reusing the same frequency to them on the same floor within a building. In line with this, authors in [26], proposed a spatial frequency reuse model for a two-tier system to exploit the advantages and limits of the mmWave frequencies. In [27], the authors proposed a novel frequency reuse method for femtocell networks by using game theory, which consists of self-organizing clustering and applying optimal frequency resource allocation to a cluster to increase the average capacity of femtocell networks. Because the individual interference from each node can be weak, contrary to the conventional graph-based frequency reuse that can mitigate the interference from individually strong interfering nodes, a hypergraph-based frequency reuse scheme in femtocell networks was proposed in [28]. The hypergraph-based frequency reuse scheme considers cumulative interference by constructing hyper-edges in the graph to capture the actual interference more accurately. With a heuristic coloring of the interference hypergraph and proportional frequency sub-band allocation, the spectrum is reused efficiently in the whole network.

To reuse any frequency to in-building SCBSs, major issues such as modeling co-channel interference (CCI) need to be addressed. Numerous existing works considered resource allocation schemes to address CCI in 3D in-building scenarios, including a semi-static resource allocation scheme in [29] and a distributed power self-optimization scheme in [30]. To address inter-femtocell interference in buildings, authors proposed a new adaptive soft frequency reuse scheme in [31], where multiple dense femtocells are classified into several groups according to the dominant interference strength to others. The minimum subchannels with different frequency reuse factors for these groups are determined and transmit powers of subchannels grouping are adaptively adjusted based on the strength to mitigate the mutual interference, which yields great spectrum efficiency compared to the legacy soft reuse. In [32], authors studied a typical in-building wireless solution using a more realistic traffic model with fixed buffer size and Poisson arrival instead of considering a full buffer traffic model. They showed that new results provide better performance for femtocells with frequency reuse one at light to medium load.

Several works also addressed interference management to reuse resources in femtocells in a 2-dimensional (2D) scenario using methods such as a game-theoretic approach in [33], an optimal static fractional frequency reuse scheme in [34], dynamic frequency management in [35], a mechanism to allocate resources to subscribed and non-subscribed users in [36], and an interference management scheme based on price in the uplink for dense femtocell systems in [37]. In [38], the authors proposed the concept of cognitive femtocell in the uplink such that the femtocell access point first senses the absence/presence of the macrocell user to maximize the femtocell throughput. If the macrocell user is sensed to be absent, the femtocell user transmits at maximum power. Otherwise, the femtocell access point optimizes the transmit power of the femtocell user.

Because the strength of CCI varies with distance, a minimum distance between co-channel SCBSs needs to be enforced [39] to maximize frequency reuse. Numerous works addressed the minimum distance enforcement between cells in the 2D scenario by employing techniques such as a base station location model in [40] using the Matern hardcore process and a repulsive cell activation strategy using a numerical search in [41]. However, CCI modeling and a minimum distance enforcement between SCBSs in a building under the 2D scenario cannot capture the impact of the third dimension, particularly, in dense urban 3D multi-story buildings. This is because, in 2D, the impact of floor attenuations, diffraction effects, and signal propagation from neighboring buildings cannot be captured, which necessitates characterizing SCBSs in 3D to reuse spectrum to in-building SCBSs. In line with this, previously, we modeled CCI and defined a minimum distance to enforce between SCBSs in each 3D multi-floor building to reuse the 2 GHz microwave spectrum in [42], 28 GHz mmWave spectrum in [43], and 140 GHz THz spectrum in [44].

C. PROBLEM STATEMENT AND CONTRIBUTIONS

A major shortcoming of [42], [43], [44] is that each considered a different path-loss model to derive CCI and minimum distance between co-channel SCBSs. This is because, to show a relative comparison in performances of different frequency bands, a *unique* path-loss model applicable for different frequencies ranging up to THz is necessary to develop a generic model to reuse different frequencies to in-building SCBSs. Unfortunately, such a generic model is not obvious in the existing literature. This paper addresses this research gap by employing a unique path-loss model termed the directional LOS 1 m close-in (CI) free space reference distance model to present a generic spectrum reuse model (GSRM) to reuse mmWave and THz frequencies to in-building SCBSs. The CI model is commonly used for large-scale path loss estimation over different frequency bands [45], [46].

It is to be noted that since mmWave and THz frequency bands are suitable for short-distance indoor communications and are also expected for next-generation mobile communications, we limit our focus in this paper mainly to mmWave and THz frequency bands even though the CI model can also be used for the microwave frequency bands. For mmWave and THz frequency bands, we consider 28 GHz, 142 GHz, 250 GHz, and 300 GHz and model CCI and derive a minimum distance to enforce between co-channel SCBSs for each mmWave and THz frequency band in each multi-story building. Note that, the paper is inspired by the observations in [42], [43], [44], including in-building interference modeling, minimum distance enforcement between small cells for the spectrum reuse, and frequency dependency of the spectrum reuse factor, leading to generating the idea of the GSRM. From this viewpoint, the paper can be considered as an extension to [46], [47], [48].

Unlike [42], each SCBS is considered to be enabled with multiple transceivers to operate on multiple mmWave and THz frequency bands simultaneously to serve more small cell capacities. Further, based on the minimum distance corresponding to any mmWave and THz frequency, a 3D cluster of apartments, or simply a 3D cluster, is defined. The same work is continuing for each mmWave and THz band. Since, in practice, an apartment in a 3D cluster may not be equipped with an SCBS, we assume a maximum of one SCBS per apartment. In other words, we assume a *random* distribution of SCBSs over a 3D cluster unlike [42], where it is considered that each apartment must have an SCBS equipped. Moreover, when the frequency of a signal increases, the distance-dependent path loss of the corresponding signal increases. Similarly, the path loss is related proportionately to the distance of the signal propagates. Hence, the 3D cluster size corresponding to any frequency band also changes for a given interference threshold. This implies that, unlike [42], [43] where the 3D cluster size is considered the same for all frequencies, we consider different 3D cluster sizes each corresponding to either a mmWave or THz frequency band to improve the utilization of mmWave and THz spectrum within in-building SCBSs. More specifically, we intend to contribute the following in this paper.

1) CONTRIBUTION 1

We present a generic spectrum reuse model (GSRM) to reuse mmWave and THz frequencies to in-building multi-band SCBSs to achieve high spectral efficiency (SE) and energy efficiency (EE) of next-generation mobile networks. In doing so, we first present a path loss model applicable to all frequencies of the multi-band SCBS. Employing the path loss model we then model the CCI of in-building small cells at both intra-floor and inter-floor levels. Subject to a CCI threshold at a small cell UE (SCUE) served by a multi-band SCBS in an apartment, a minimum distance between the SCUE and each co-channel interferer at both intra-and inter-floor levels in a multi-floor building is derived for each frequency band. A 3D cluster and hence the spectrum reuse factor within the building are derived for each band, representing the number of times the corresponding band can be reused to SCBSs of each 3D cluster within the building. The spectrum reuse factor is further explored for two cases, depending on the existence of an SCBS in an apartment, i.e., whether or not each apartment in a 3D cluster is equipped with an SCBS.

2) CONTRIBUTION 2

An analytical model is then developed to derive SE and EE performance metrics of GSRM in a multi-tier network consisting of an outdoor macrocell, a set of picocells, and indoor small cells.

3) CONTRIBUTION 3

We develop an algorithm of the proposed GSRM under two scenarios, depending on whether the same (scenario 1) or a different (scenario 2) size of the 3D cluster is considered for each frequency band of an SCBS for both static and random distributions of small cells per 3D cluster.

4) CONTRIBUTION 4

We carry out extensive system-level performance evaluations and assess numerous performance attributes, including the impact of the interference threshold on the spectrum reuse factor, the average capacity per SCUE, the effect of variation in the spectrum reuse factor on SE and EE at each band, and the impact of small cells when enabled with a single band and multiple bands on SE and EE metrics. Besides, for multi-band-enabled small cells, we evaluate the relative performance of scenario 1 with scenario 2 in terms of overall SE and EE per building. Finally, we present whether or not the proposed GSRM can achieve the prospective SE and EE performances required for the 6G mobile system.

D. ORGANIZATION

The paper is organized as follows. In Section II, CCI modeling in small cell networks in a 3D in-building scenario is presented. Particularly, we introduce a multi-tier network architecture, discuss CCI modeling in a 3D in-building multi-band small cell network, and discuss the impact of the 3D cluster size and the existence of a small cell per apartment in each 3D cluster at different mmWave and THz frequency bands. The proposed GSRM for reusing mmWave and THz spectrum to small cells located in 3D multi-story buildings is presented in Section III. CCI is formulated at both inter-floor and inter-floor levels and a minimum distance between co-channel in-building SCBSs is derived to develop a 3D cluster. Section IV presents an analytical model of a multi-tier network and derives relevant SE and EE performance metrics to assess the performance of the proposed GSRM. An algorithm is then developed and pertaining simulation parameters and assumptions are highlighted in Section V. Moreover, issues such as floor penetration loss, inter-wall penetration loss, multi-band small cells, and the impact of

TABLE 1. List of abbreviations.

Abbreviation	Full form
2G	Second-Generation
3D	3-Dimensional
3G	Third-Generation
3GPP	3rd Generation Partnership Project
4G	4th Generation
5G	Fifth-Generation
6G	Sixth-Generation
CCI	Co-Channel Interference
CI	Close-In
CIF	CI Model with a Frequency-Weighted PLE
CSG	Closed Subscriber Group
dB	Decibels
GSRM	Generic Spectrum Reuse Model
LOS	Line-of-Sight
LTE	Long Term Evolution
MCBS	Macrocell Base Station
MIMO	Multiple-Input Multiple-Output
mmWave	Millimeter wave
MNO	Mobile Network Operator
NLOS	Non-Line-of-Sight
PCBS	Picocell Base Station
PF	Proportional Fair
PLE	Path Loss Exponent
RB	Resource Block
RF	Reuse Factor
RoE	Region of Exclusion
SCBS	Small Cell Base Station
SCUE	Small Cell UE
THz	Terahertz
TTI	Transmission Time Interval
UE	User Equipment
WRC	World Radiocommunication Conference

small cells of adjacent buildings are clarified. In Section VI, the SE and EE metrics of the GSRM are evaluated under numerous attributes, particularly the impact of interference threshold on spectrum reuse factor, path loss analysis at high frequencies, as well as spectrum reuse in small cells for scenario 1 and scenario 2. Finally, we show whether or not the proposed GSRM can satisfy the prospective SE and EE performances of the 6G mobile system. We conclude the paper in Section VII. Table 1 shows a list of abbreviations.

II. INTERFERENCE MODELING IN 3D IN-BUILDING SMALL CELL NETWORKS

A. SYSTEM ARCHITECTURE OF A MULTI-TIER NETWORK

Fig. 1(a) shows the system architecture of a multi-tier network, comprising a macrocell along with several picocells and femtocells also termed small cells located within the coverage of the macrocell. Picocells are deployed outdoors, whereas, small cells are deployed indoors within several multi-floor buildings. We consider a multi-floor building as shown in Fig. 1(b) that comprises a maximum of F_{max} floors such that $N \in F = \{1, 2, 3, \ldots, F_{\max}\}$. Each floor (Fig. 1(c)) has the same number of apartments. Complying with the practical scenario, we assume each apartment is square having a side length of 10 meters and a height of 3 meters. Assume a free space of 10 meters around the building [47], [48]. However, in general, the side length, the height of an apartment, and the free space around the building are random variables. Note that though the hexagonal cell shape can cover the maximum area, we choose alternative small cell shapes, i.e., square shape, to ensure no gap and overlapping between adjacent small cells to comply with the shape of a practical apartment in a 3D building.

We assume a maximum of one SCBS per apartment, equipped with multiple transceivers, operating at a different mmWave and THz frequency, to serve high data rates for indoor traffic. Specifically, we consider four transceivers, operating at 28 GHz mmWave and 142 GHz, 250 GHz, and 300 GHz THz frequencies, for each SCBS as shown in Fig. 1(d). Each SCBS is installed on the midpoint of the ceiling of each square apartment within the building. We consider only one SCUE per SCBS (also called serving SCBS), which is placed at the farthest radial distance of 5 meters horizontally and a maximum height of 3 meters vertically from the floor of an apartment for the worst-case scenario.

UEs that are served by the macrocell base station (MCBS) are classified as macrocell UEs. Macrocell UEs may exist in both outdoor and indoor environments and hence are classified further as outdoor macrocell UEs and indoor macrocell UEs, respectively. Note that, as a default scenario, an indoor macrocell UE is served by the MCBS if it is not served by any in-building SCBS. Further, we assume that, at any instant in time, a certain percentage of outdoor macrocell UEs are offloaded to nearby picocells to receive better signal strengths. Macrocell UEs that are offloaded to any picocell base station (PCBS) are served by the corresponding PCBS and are classified as picocell UEs. Hence, the total number of macrocell UEs is the sum of indoor macrocell UEs, outdoor macrocell UEs, and picocell UEs. For SCBSs, we consider Closed Subscriber Group (CSG) femtocell base stations, which are implemented by users. Hence, only a SCUE that is subscribed to an SCBS, can be served by the corresponding SCBS as long as the SCUE is within the coverage of the SCBS. When the SCUE is out of the SCBS's coverage, it will be served by the MCBS. Note that since the MCBS operates at the microwave frequency, each SCUE must be equipped with a separate transceiver operating at the microwave frequency of the MCBS in addition to that of mmWave and THz frequencies.

Remark 1 (SCUEs Per SCBS): For the resource block (RB) allocation, we consider the Proportional Fair (PF) scheduler that allocates RBs orthogonally to in-building small cell UEs. For any variation in the number of UEs served by an SCBS at any transmission time interval (TTI), the PF scheduler simply updates the number of RBs to be allocated to the SCBS commensurate with its new traffic demand to be served. For a given bandwidth, this change in the number of SCUEs over time served by any SCBS does not affect the overall aggregate capacity, and hence other related performance metrics, including SE and EE noticeably. This can be clarified by the fact that the total number of RBs, which is fixed for a given bandwidth, is simply rescheduled among the predefined group of in-building SCBSs following the new traffic demand (due to the change in the number

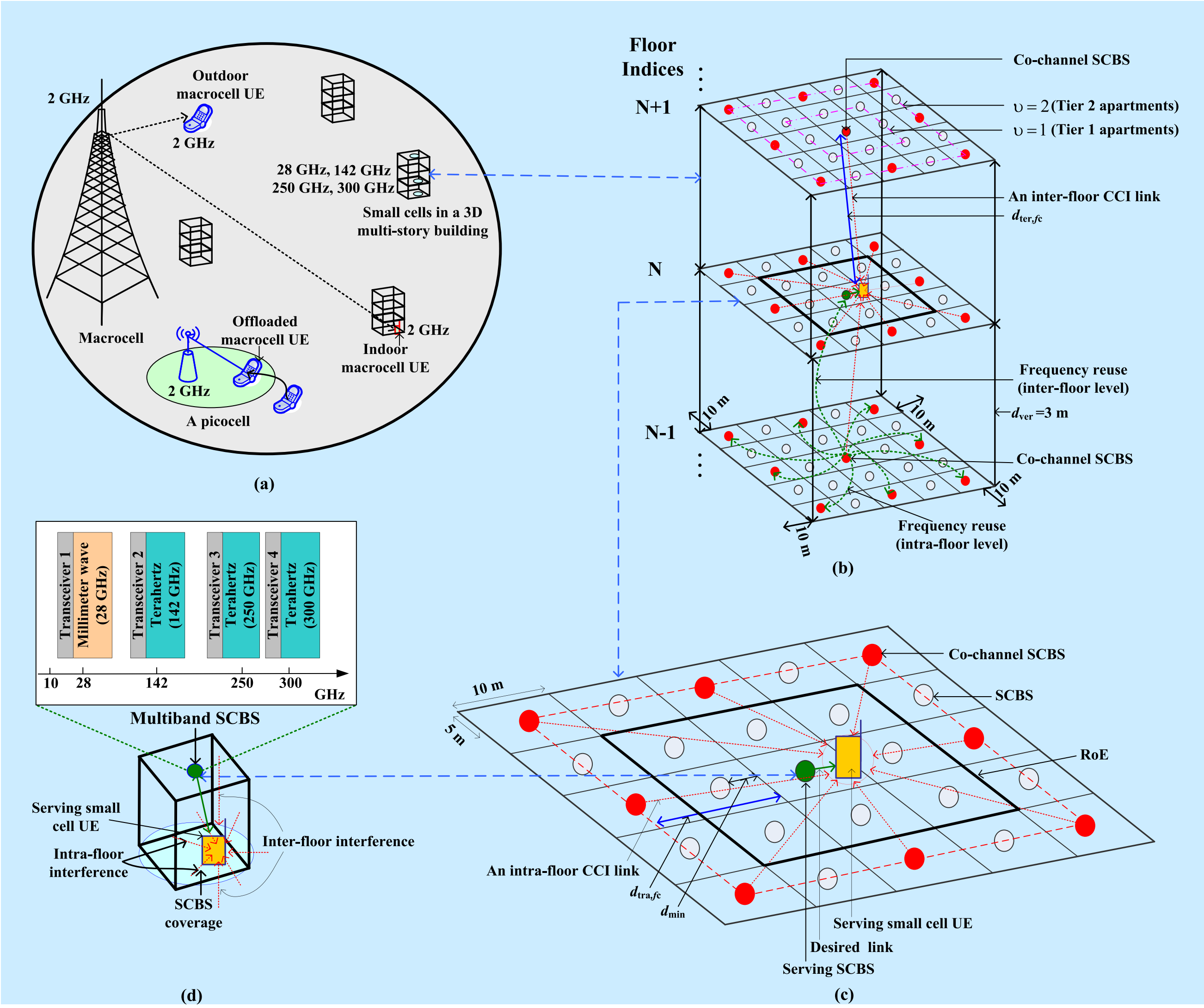

FIGURE 1. **(a) System architecture of a multi-tier network; (b) Interference modeling in a 3D in-building small cell network; (c) Interference modeling in a 2D intra-floor in-building small cell network (d) a multi-band SCBS.**

of SCUEs) of each SCBS in the group. Because the indoor channel characteristics of SCBSs do not vary considerably from one TTI to another, the change in overall performances, in terms of, for example, aggregate capacity, SE, and EE is insignificant with a change in the number of SCUEs per SCBS. That's why, we avoid considering multiple SCUEs served concurrently by an SCBS and instead, we consider only one SCUE can be served at a time by an SCBS for simplicity in analysis. Note that, the same assumption as one SCUE per SCBS has also been adopted in the existing literature, for example [49], [50].

B. INTERFERENCE MODELING IN 3D IN-BUILDING SMALL CELL NETWORKS

This section presents a detailed explanation of interference modeling for the spectrum reuse in a multistory building, including the number of apartments per floor, placement of SCBS and SCUE per apartment, location of co-channel interferers at both intra-floor and inter-floor levels, depiction of a minimum distance between co-channel SCBSs at both intra-and inter-floor levels, and formation of a 3D region of exclusion (RoE). We capture the interference modeling in a 3D in-building small cell network in Fig. 1(b). The link between the serving SCUE and the serving SCBS is called the *desired link*, whereas, the link between the serving SCUE and any co-channel SCBS is called the *CCI link*. Co-channel SCBSs for a serving SCUE on any floor may exist where the intra-floor level implies that both the serving SCUE and the co-channel SCBS are located on the same floor (Fig. 1(c)), and the inter-floor level implies that the serving SCUE and co-channel SCBS are located on different floors (Fig. 1(b)). The planer-Wyner model is used to model the intra-floor CCI [51], whereas, the linear-Wyner model to model the inter-floor CCI.

Depending on the maximum allowable CCI, also termed interference threshold, at a serving SCUE, the locations of the co-channel interferers at both intra-and inter-floor levels vary. However, irrespective of the locations of co-channel SCBSs from the serving SCBS, a maximum of eight, whereas a maximum of two, co-channel SCBSs for a serving SCUE in each tier of co-channel SCBSs exist. From Fig. 1(b), even though the distance of all co-channel SCBSs from a serving SCUE is not the same, for simplicity in modeling, we assume each co-channel SCBS in the same tier is located at the same distance from the serving SCUE.

Note that because of a low transmit power and high partition loss at the intra-floor level or high floor penetration loss at the inter-floor level, the overall impact of co-channel SCBSs in higher tiers is considered insignificant, leading us to consider only the first-tier of co-channel SCBSs sufficient enough to reduce complexity in evaluation. In Fig. 1(b), no reuse of the same resources can be possible in SCBSs surrounded by the first tier of co-channel SCBSs. The region of SCBSs with no resource reuse permitted is called the 3D RoE or 3D cluster of SCBSs [42] at both intra-and inter-floor levels. In general, the larger the area of RoE, the lower the CCI effect at the serving SCUE and vice versa. Hence, the RoE at both the intra-and inter-floor levels depends on the minimum distance addressing the minimum CCI constraint between the serving SCUE and any co-channel SCBS on the same tier. In other words, changing the maximum allowable CCI at the serving SCUE, the RoE, and correspondingly, the spectrum reuse factor can be varied.

In Fig. 1(b), the SCBS in green represents the serving SCBS, SCBSs in red circles within square apartments represent co-channel SCBSs, and a group of SCBSs around the serving SCBS surrounded by the thick black line represents RoE. In Fig. 1(d), the line in green represents the desired link from serving SCBS to serving SCUE, and the lines in red represent CCI links. Also, solid lines in blue represent the minimum distances between any co-channel SCBS and the serving SCUE at both intra-floor (Fig. 1(c)) and inter-floor (Fig. 1(b)) levels.

C. IMPACT OF CLUSTER SIZES AND SCBSS

Usually, the 3D cluster size reduces with an increase in frequency. Hence, in a multi-band SCBS, the spectrum reuse factor of high frequencies is reduced if we assume the same cluster size. Usually, the cluster size as that of the lowest frequency is considered for all the frequencies of the SCBS to ensure that the interference threshold and hence the minimum distance requirement at both intra-floor and inter-floor levels for each frequency band is satisfied. However, reducing the spectrum reuse factor reduces spectrum utilization, decreasing spectral and energy efficiencies of high frequencies in a multi-band SCBS.

We depict an example of scenario 1 and scenario 2 in Fig. 2 (without proofs) of a multi-band SCBS operating at 28 GHz, 142 GHz, 250 GHz, and 300 GHz bands. 28 GHz and 142 GHz correspond to a minimum distance requirement that requires a 2D cluster at the intra-floor level of 49 SCBSs (shown in a green thick line), whereas 250 GHz and 300 GHz correspond to a minimum distance requirement that requires a 2D cluster of 25 SCBSs (shown in a blue thick line). This implies that 250 GHz and 300 GHz can be reused more than 28 GHz and 142 GHz of the SCBS.

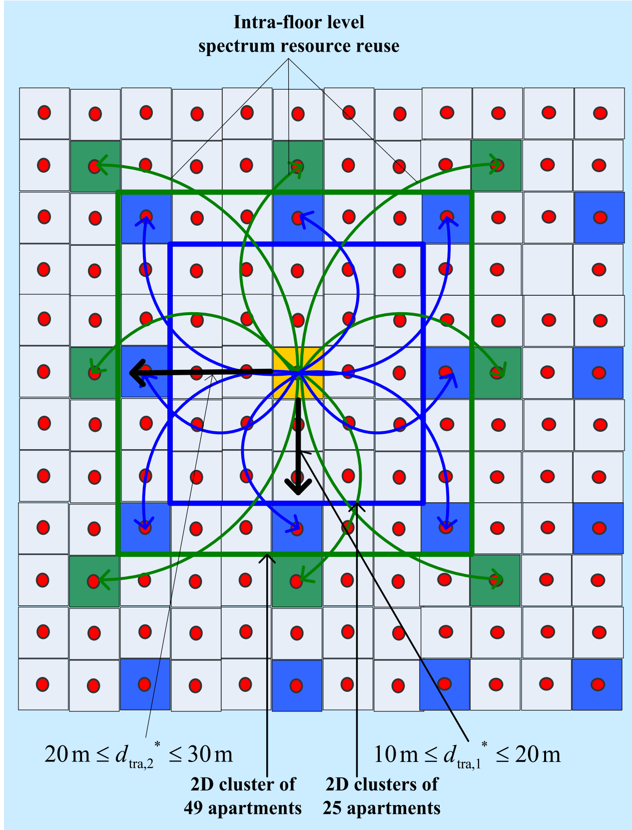

FIGURE 2. Scenario 1 where the 2D cluster is defined by $20\ m \leq d_{tra}^{*} \leq 30$ m corresponding to only the minimum frequency band (e.g., 28 GHz) is employed to reuse spectrum resources. Scenario 2 where 2D clusters are defined by both 20 m $\leq d_{tra}^{*} \leq 30$ m (e.g., for 28 GHz and 142 GHz) and $10\ m \leq d_{tra}^{*} \leq 20$ m (250 GHz and 300 GHz), corresponding to different frequency bands employed to reuse spectrum resources.

Hence, from the spectrum utilization perspective, scenario 2 is preferable to scenario 1. This, however, comes at the cost of additional complexities due to redefining a 3D cluster for each frequency band. So, we consider two scenarios where in scenario 1, the 3D cluster for all frequencies of a multi-band SCBS is defined by the (same) minimum frequency of all, and in scenario 2, 3D clusters for all frequencies are defined corresponding to their respective frequency bands. We evaluate both scenarios with an extensive system-level simulation in the following sections.

Moreover, in practice, each apartment in a 3D cluster may not have an SCBS installed. So, we examine two cases where in case 1, we assume one SCBS per apartment, and in case 2, we assume a certain percentage of SCBSs within a 3D cluster do not have an SCBS installed as shown in Fig. 3(a), and Fig. 3(b), respectively.

Case 1 assumes an ideal scenario and can be applicable if considering open access femtocell base stations for SCBSs. This is because open access femtocell base stations are installed by the mobile network operator, and it is not uncommon that an operator may plan to install an open access femtocell base station in each apartment of a multi-floor building to serve high capacity and data rate demands in indoor environments. Case 1 may also apply to some extent to hybrid access femtocell base stations where some channels of a femtocell base station are restricted only to the user (owner of the apartment) and the remaining channels of the femtocell can be accessed by any user of the network operator. Hybrid access femtocells can be deployed either by the user or by the network operator depending on how both parties agree to the hybrid access.

Case 1, however, cannot be guaranteed if CSG femtocell base stations, which are installed by users, are considered for SCBSs. This is because, in practice, a user may not be willing to install a femtocell base station in his/her apartment. This results in considering case 2, which assumes random placement of SCBSs per apartment, meaning that the number of SCBSs of one 3D cluster differs from another in a building. More specifically, in case 2, we assume a random distribution in the installment of an SCBS per apartment within a 3D cluster, not a random distribution of the installment of an SCBS within the coverage of each apartment. We are not concerned with the distribution of an SCBS (i.e., how an SCBS is placed) within an apartment. We rather consider that the placement of an SCBS if installed in an apartment is fixed on the midpoint of the ceiling of the corresponding apartment. No matter which of the three modes of operation of the femtocell base station is selected, case 1 and case 2 are sufficient to capture the probable SCBS deployment for spectrum reuse in a multi-floor building scenario.

III. GENERIC MMWAVE AND THZ SPECTRUM REUSE MODEL FOR IN-BUILDING SMALL CELLS

This section presents the proposed GSRM for reusing mmWave and THz frequency spectrums in small cells located in 3D multi-story buildings. The path loss model used to model CCI is first discussed. CCIs are then modeled, and a minimum distance between co-channel SCBSs at both intra- and inter-floor levels is derived to define a 3D cluster. The entire mmWave and THz frequency spectrums are assigned to SCBSs within each 3D cluster as long as the spectrum covers all the SCBSs within a multi-story building.

A. PATHLOSS MODEL

The coverage of radio signals at high frequencies such as mmWave and THz is limited because of the huge path loss in the first meter. However, due to its highly directive beamforming characteristic, such path loss at high frequencies can be overcome by employing directional antennas [51], [52], [53], [54]. Hence, to estimate the path loss over a single frequency, we consider employing the directional LOS *1 m CI free space reference distance model*, which is commonly used as well for large-scale path loss estimation over different frequency bands [45], [46] given as follows

$$PL^{\mathrm{CI}} = \mathrm{FSPL}(f_{\mathrm{c}}, 1 \quad \mathrm{m}) + 10n\log_{10}\left(\frac{d_{3\mathrm{D}}}{1\mathrm{m}}\right) + X_{\sigma}, \quad (1)$$

such that

$$\mathrm{FSPL}(f_c, \quad 1 \mathrm{\ m}) = 32.4 + 20\log_{10}\left(\frac{f_c}{1 \mathrm{\ GHz}}\right), \quad (2)$$

where $d_{3\mathrm{D}}$ denotes the distance in 3D between transmit and receive antennas, f_{c} denotes any mmWave and THz frequencies, including 28 GHz, 142 GHz, 250 GHz, and 300 GHz, i.e., $f_{\mathrm{c}} \in \{28, 142, 250, 300\}$, $\mathrm{FSPL}(f_c, 1 \mathrm{\ m})$ denotes the free space path loss at f_{c}, n denotes the path loss exponent (PLE), X_{σ} denotes the shadow fading in dB, which is defined as a zero mean Gaussian random variable with a standard deviation σ in dB [45], [46], [53], [54], [55], [56], [57], [58], [59]. Table 2 shows PLE and the effect of shadowing at 28 GHz, 142 GHz, 250 GHz, and 300 GHz.

TABLE 2. Channel parameters of the CI path loss model in the directional indoor hotspot (InH)-office [52].

Frequency type f_c (GHz)	28	142	250	300
PLE (n_{f_c})	1.90	2.05	2.27	2.32
Shadow fading (dB)	3.38	2.89	3.06	4.05

The above single-band CI model in (1) can be extended to a multi-band model for indoor environments by introducing a frequency-weighted PLE (CIF) [45], [60] to (1) using Table 2, offering an additional degree of freedom over a wide range of frequencies. Hence, the CI path loss model (1) can also be used as a multi-band path loss model, using only a single parameter PLE [55], [60], [61].

Remark 2 (Pathloss Models): In [52], it is shown that both CI and CIF demonstrate notable similarity in terms of PLEs over 28 GHz, 73 GHz, and 142 GHz when referencing the free space reference distance of the 1st meter [55], [60], [61]. This implies that additional parameters in the CIF may not be essential over wide frequency bands, demonstrating that an identical PLE may model the path loss accurately over a wide range of frequencies by considering the pathloss in the 1st meter of propagation as the only frequency-dependent effect [53], [55], [60], [61]. Due to its validity over a large frequency spectrum, we use the single-band path loss CI model (directional) for all mmWave and THz frequencies from 10 to 330 GHz [52] to model in-building CCI at intra- and inter-floor levels for mmWave and THz frequencies in the following section.

B. MODELING IN-BUILDING CO-CHANNEL INTERFERENCE OF SMALL CELL NETWORKS

1) INTRA-FLOOR CCI

In general, considering the partition loss and shadowing effect, the normalized value of the intra-floor CCI experienced by the serving SCUE because of any co-channel

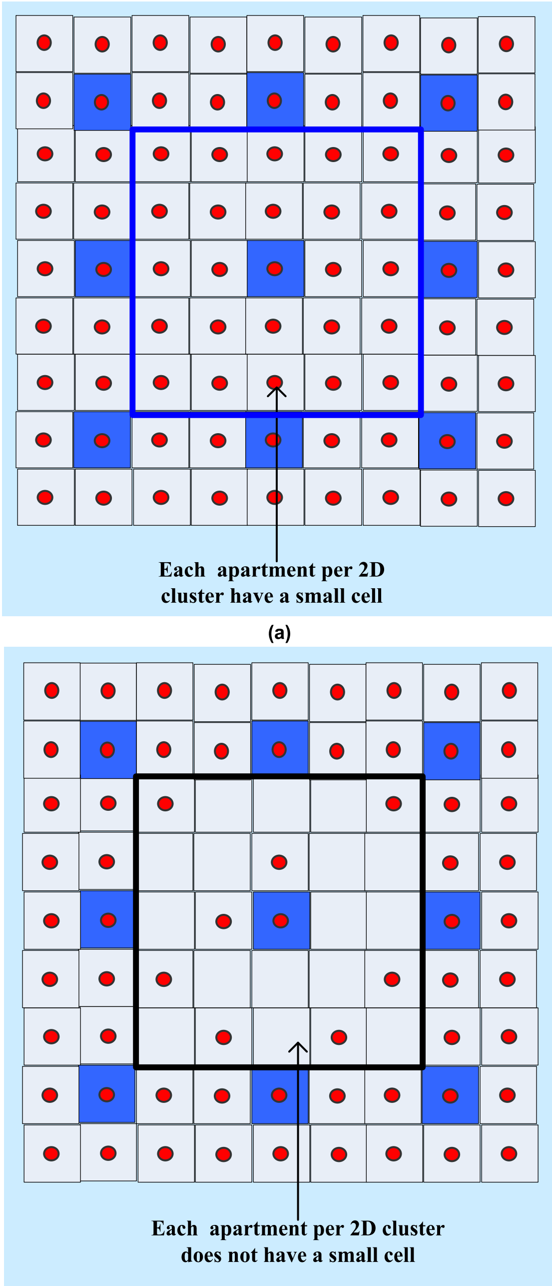

FIGURE 3. (a) Each apartment per 2D cluster has a small cell; (b) Each apartment per 2D cluster does not have a small cell.

interferer situated at a distance $d_{\mathrm{tra,f_c}}$ at f_c can be expressed as follows

$$\alpha_{\mathrm{tra}}^{\mathrm{nor}}\left(d_{\mathrm{tra},\ f_c}\right) = \left[10^{\left(\left(X_{d_{\min}}^{f_c} - X_{d_{\mathrm{tra}}}^{f_c} + \beta_{d_{\min}}^{f_c} - \beta_{d_{\mathrm{tra}}}^{f_c}\right)/10\right)}\right] \times \left(\frac{d_{\min}}{d_{\mathrm{tra},\ f_c}}\right)^{n_{f_c}}. \tag{3}$$

Proof: See Proof 1.

Proof 1: Let $\beta_{d_{\mathrm{tra}}}^{f_c}$ denote the partition loss between a co-channel interferer and a serving SCUE. The received intra-floor CCI at the SCUE when operating f_c in GHz can be expressed as follows

$$\alpha_{\mathrm{tra}}\left(d_{\mathrm{tra},\ f_c}\right)[\mathrm{dB}] = P_{Tx,\ f_c}^{\mathrm{SC}} - \left(\mathrm{PL}_{f_c}^{\mathrm{CI}} + \beta_{d_{\mathrm{tra}}}^{f_c}\right)$$

$$\alpha_{\mathrm{tra}}\left(d_{\mathrm{tra},\ f_c}\right)[\mathrm{dB}] = P_{TX,\ f_c}^{\mathrm{SC}} - \left(\begin{array}{c}\mathrm{FSPL}(f_c,\ 1\ \mathrm{m}) + \\ 10\ n_{f_c}\log_{10}\left(d_{\mathrm{tra},\ f_c}\right) + X_{d_{\mathrm{tra}}}^{f_c} + \beta_{d_{\mathrm{tra}}}^{f_c}\end{array}\right).$$

When expressed in the absolute value from the dB, after manipulating the above equation, the CCI from any intra-floor co-channel interferer at f_c is given by

$$\alpha_{\mathrm{tra}}\left(d_{\mathrm{tra},\ f_c}\right) = 10^{0.1\times\left(P_{TX,\ f_c}^{\mathrm{SC}} - \left(\begin{array}{c}\mathrm{FSPL}(f_c,\ 1\ \mathrm{m}) + \\ 10\ n_{f_c}\log_{10}\left(d_{\mathrm{tra},\ f_c}\right) + X_{d_{\mathrm{tra}}}^{f_c} + \beta_{d_{\mathrm{tra}}}^{f_c}\end{array}\right)\right)}.$$

Because of the high internal wall attenuation experienced by mmWave signals, and the low transmission power of a small cell, it is sufficient to consider only the first-tier intra-floor interferers' effect for a serving SCUE. Further, under the worst-case, CCI experienced by a serving SCUE is the maximum when any intra-floor interferer operating at f_c is situated at a distance $d_{\mathrm{tra},\ f_c} = d_{\min}$ and can be expressed as follows

$$\alpha_{\mathrm{tra}}^{\max}\left(d_{\mathrm{tra},\ f_c}\right) = 10^{0.1\times\left(P_{TX,\ f_c}^{\mathrm{SC}} - \left(\begin{array}{c}\mathrm{FSPL}(f_c,\ 1\ \mathrm{m}) + \\ 10\ n_{f_c}\log_{10}(d_{\min}) + X_{d_{\min}}^{f_c} + \beta_{d_{\min}}^{f_c}\end{array}\right)\right)},$$

where $\beta_{d_{\min}}^{f_c}$ denotes the partition loss and $X_{d_{\min}}^{f_c}$ denotes the shadowing effect to the SCUE from its closest co-channel interferer at $d_{\mathrm{tra},\ f_c} = d_{\min}$. Hence, the normalized value of the CCI from any intra-floor co-channel interferer at the SCUE at f_c is given by

$$\alpha_{\mathrm{tra}}^{\mathrm{nor}}\left(d_{\mathrm{tra},\ f_c}\right) = \alpha_{\mathrm{tra}}\left(d_{\mathrm{tra},\ f_c}\right)/\alpha_{\mathrm{tra}}^{\max}\left(d_{\mathrm{tra},\ f_c}\right) \tag{4}$$

$$\alpha_{\mathrm{tra}}^{\mathrm{nor}}\left(d_{\mathrm{tra},\ f_c}\right) = 10^{\left(\begin{array}{l}0.1\times\left(P_{TX,\ f_c}^{\mathrm{SC}} - \left(\mathrm{FSPL}(f_c,\ 1\ \mathrm{m}) + 10\ n_{f_c}\log_{10}\left(d_{\mathrm{tra},\ f_c}\right) + X_{d_{\mathrm{tra}}}^{f_c} + \beta_{d_{\mathrm{tra}}}^{f_c}\right)\right) \\ -0.1\times\left(P_{TX,\ f_c}^{\mathrm{SC}} - \left(\mathrm{FSPL}(f_c,\ 1\ \mathrm{m}) + 10\ n_{f_c}\log_{10}(d_{\min}) + X_{d_{\min}}^{f_c} + \beta_{d_{\min}}^{f_c}\right)\right)\end{array}\right)}$$

$$\alpha_{\mathrm{tra}}^{\mathrm{nor}}\left(d_{\mathrm{tra},\ f_c}\right) = 10^{\left(\begin{array}{l}0.1\times\left(P_{TX,\ f_c}^{\mathrm{SC}} - \left(\mathrm{FSPL}(f_c,\ 1\ \mathrm{m}) + 10\ n_{f_c}\log_{10}\left(d_{\mathrm{tra},\ f_c}\right) + X_{d_{\mathrm{tra}}}^{f_c} + \beta_{d_{\mathrm{tra}}}^{f_c}\right)\right) \\ 0.1\times\left(-P_{TX,\ f_c}^{\mathrm{SC}} + \left(\mathrm{FSPL}(f_c,\ 1\ \mathrm{m}) + 10\ n_{f_c}\log_{10}(d_{\min}) + X_{d_{\min}}^{f_c} + \beta_{d_{\min}}^{f_c}\right)\right)\end{array}\right)}$$

$$\alpha_{\mathrm{tra}}^{\mathrm{nor}}\left(d_{\mathrm{tra},\ f_c}\right) = 10^{\left(\begin{array}{l}-0.1\times\left(10\ n_{f_c}\log_{10}\left(d_{\mathrm{tra},\ f_c}\right) + X_{d_{\mathrm{tra}}}^{f_c} + \beta_{d_{\mathrm{tra}}}^{f_c}\right) \\ +0.1\times\left(10\ n_{f_c}\log_{10}(d_{\min}) + X_{d_{\min}}^{f_c} + \beta_{d_{\min}}^{f_c}\right)\end{array}\right)}$$

$$\alpha_{\mathrm{tra}}^{\mathrm{nor}}\left(d_{\mathrm{tra},\ f_c}\right) = 10^{\left(\begin{array}{l}-n_{f_c}\log_{10}\left(d_{\mathrm{tra},\ f_c}\right) \\ +n_{f_c}\log_{10}(d_{\min})\end{array}\right)} 10^{\left(\begin{array}{l}-0.1\times\left(X_{d_{\mathrm{tra}}}^{f_c} + \beta_{d_{\mathrm{tra}}}^{f_c}\right) \\ +0.1\times\left(X_{d_{\min}}^{f_c} + \beta_{d_{\min}}^{f_c}\right)\end{array}\right)}$$

$$\alpha_{\mathrm{tra}}^{\mathrm{nor}}\left(d_{\mathrm{tra},\ f_c}\right) = 10^{\log_{10}\left(\frac{d_{\min}}{d_{\mathrm{tra},\ f_c}}\right)^{n_{f_c}}} 10^{\left(\begin{array}{l}-0.1\times\left(X_{d_{\mathrm{tra}}}^{f_c} + \beta_{d_{\mathrm{tra}}}^{f_c}\right) \\ 0.1\times\left(X_{d_{\min}}^{f_c} + \beta_{d_{\min}}^{f_c}\right)\end{array}\right)}$$

$$\alpha_{\text{tra}}^{\text{nor}}(d_{\text{tra},\,f_c}) = \left[10^{\left(\frac{\left(X_{d_{\min}}^{f_c} - X_{d_{\text{tra}}}^{f_c} + \beta_{d_{\min}}^{f_c} - \beta_{d_{\text{tra}}}^{f_c}\right)}{10}\right)}\right] \times \left(\frac{d_{\min}}{d_{\text{tra},\,f_c}}\right)^{n_{f_c}}. \tag{5}$$

If the shadowing effect is considered the same for all links indoors, the above equation simplifies to the following

$$\alpha_{\text{tra}}^{\text{nor}}(d_{\text{tra},\,f_c}) \cong \left[10^{\left(\left(\beta_{d_{\min}}^{f_c} - \beta_{d_{\text{tra}}}^{f_c}\right)/10\right)}\right] \times \left(\frac{d_{\min}}{d_{\text{tra},\,f_c}}\right)^{n_{f_c}}. \tag{6}$$

The above equation can be further simplified to the following if the *partition loss* is assumed to be the same for all co-channel interferer links

$$\alpha_{\text{tra}}^{\text{nor}}(d_{\text{tra},\,f_c}) \cong \left(\frac{d_{\min}}{d_{\text{tra},\,f_c}}\right)^{n_{f_c}}. \tag{7}$$

Note that equation (5) gives an accurate result for the intra-floor interference by explicitly incorporating the shadowing effect and partition loss for each co-channel interferer link by measuring each CCI signal strength at the serving SCUE with a proper experimental setup. This, however, will impose additional complexities in evaluating intra-floor CCI. More simplistic expressions for the intra-floor interference can be derived as given by (6) and (7) by assuming a similar shadowing effect and partition loss for each link in (5) such that their overall impact can be neglected.

2) INTER-FLOOR CCI

Considering the floor penetration loss and the shadowing effect, the normalized inter-floor CCI power experienced by the serving SCUE due to a co-channel interferer situated at a distance d_{ter,f_c} away from the corresponding UE at any frequencyf_{c}can be expressed as follows

$$\alpha_{\text{ter}}^{\text{nor}}(d_{\text{ter},\,f_c}) = \left[10^{\left(\left(X_{d_{\min}}^{f_c} - X_{d_{\text{ter}}}^{f_c} + \gamma_{d_{\min}}^{f_c} - \gamma_{d_{\text{ter}}}^{f_c}\right)/10\right)}\right] \times \left(\frac{d_{\min}}{d_{\text{ter},\,f_c}}\right)^{n_{f_c}}. \tag{8}$$

3) PROOF. SEE PROOF 2.

Proof 2: Let $d_{\text{ter},\,f_c}$ denote the distance of a co-channel SCBS from the serving SCUE at f_c and $d_{\text{ter},\,f_c} = \sqrt{{d_{\min}}^2 + {d_{\text{ver}}}^2}$, where d_{ver} denotes the vertical distance between the serving SCBS and any co-channel SCBS on a floor other than that of the serving SCBS. Now, following (3), the inter-floor CCI power can be expressed similarly by incorporating a floor penetration loss $\gamma_{d_{\text{ter}}}^{f_c}$ instead of the partition loss as in the case of the intra-floor CCI. The received inter-floor CCI power at the SCUE due to any inter-floor co-channel interferer situated at a distance $d_{\text{ter},\,f_c}$ away from the corresponding SCUE at any frequency f_c can be given by

$$\alpha_{\text{ter}}(d_{\text{ter},\,f_c})[\text{dB}] = P_{\text{Tx},\,f_c}^{\text{SC}} - \left(\text{PL\_}{f_c}^{\text{CI}} + \gamma_{d_{\text{ter}}}^{f_c}\right)$$

$$\alpha_{\text{ter}}(d_{\text{ter},\,f_c})[\text{dB}] = P_{\text{TX},\,f_c}^{\text{SC}} - \left(\begin{array}{c}\text{FSPL}(f_c, 1\text{ m}) + \\ 10\, n_{f_c} \log_{10}(d_{\text{ter},\,f_c}) + X_{d_{\text{ter}}}^{f_c} + \gamma_{d_{\text{ter}}}^{f_c}\end{array}\right).$$

When expressed in the absolute scale from the dB scale, after manipulating the above equation, the CCI effect at the serving SCUE due to inter-floor co-channel interferers of the first-tier situated on different floors from that of the serving SCUE can be given by

$$\alpha_{\text{ter}}(d_{\text{ter},\,f_c}) = 10^{0.1\times\left(P_{\text{TX},\,f_c}^{\text{SC}} - \left(\begin{array}{c}\text{FSPL}(f_c, 1\text{ m}) + \\ 10\, n_{f_c} \log_{10}(d_{\text{ter},\,f_c}) + X_{d_{\text{tra}}}^{f_c} + \gamma_{d_{\text{ter}}}^{f_c}\end{array}\right)\right)}.$$

For the worst-case scenario, inter-floor CCI power is the maximum and can be expressed as follows

$$\alpha_{\text{ter}}^{\max}(d_{\text{ter},\,f_c} = d_{\min}) = 10^{0.1\times\left(P_{\text{TX},\,f_c}^{\text{SC}} - \left(\begin{array}{c}\text{FSPL}(f_c, 1\text{ m}) + \\ 10\, n_{f_c} \log_{10}(d_{\min}) + X_{d_{\min}}^{f_c} + \gamma_{d_{\min}}^{f_c}\end{array}\right)\right)}, \tag{9}$$

where $\gamma_{\min}^{f_c}$ denotes the (minimum) floor penetration loss and $X_{d_{\text{ter}}}^{f_c}$ denotes the shadow fading effect on an inter-floor link between the serving SCUE and its closest inter-floor interferer. The term minimum for the floor penetration loss implies that the number of floors from the closest co-channel interferer to the serving SCUE is the minimum, compared to other co-channel interferers. Hence, the normalized CCI from any inter-floor interferer at the serving SCUE at any frequency f_c is given by

$$\alpha_{\text{ter}}^{\text{nor}}(d_{\text{ter},\,f_c}) = \alpha_{\text{ter}}(d_{\text{ter},\,f_c}) / \alpha_{\text{ter}}^{\max}(d_{\text{ter},\,f_c})$$

$$\alpha_{\text{ter}}^{\text{nor}}(d_{\text{ter},\,f_c}) = 10^{\left(\begin{array}{l} 0.1\times\left(P_{TX,\,f_c}^{\text{SC}} - \left(\text{FSPL}(f_c, 1\text{ m}) + 10\, n_{f_c}\log_{10}(d_{\text{ter},\,f_c}) + X_{d_{\text{ter}}}^{f_c} + \gamma_{d_{\text{ter}}}^{f_c}\right)\right) \\ -0.1\times\left(P_{TX,\,f_c}^{\text{SC}} - \left(\text{FSPL}(f_c, 1\text{ m}) + 10\, n_{f_c}\log_{10}(d_{\min}) + X_{d_{\min}}^{f_c} + \gamma_{d_{\min}}^{f_c}\right)\right)\end{array}\right)}$$

$$\alpha_{\text{tra}}^{\text{nor}}(d_{\text{ter},\,f_c}) = 10^{\left(\begin{array}{l} 0.1\times\left(P_{TX,\,f_c}^{\text{SC}} - \left(\text{FSPL}(f_c, 1\text{ m}) + 10\, n_{f_c}\log_{10}(d_{\text{ter},\,f_c}) + X_{d_{\text{ter}}}^{f_c} + \gamma_{d_{\text{ter}}}^{f_c}\right)\right) \\ +0.1\times\left(-P_{TX,\,f_c}^{\text{SC}} + \left(\text{FSPL}(f_c, 1\text{ m}) + 10\, n_{f_c}\log_{10}(d_{\min}) + X_{d_{\min}}^{f_c} + \gamma_{d_{\min}}^{f_c}\right)\right)\end{array}\right)}$$

$$\alpha_{\text{ter}}^{\text{nor}}(d_{\text{ter},\,f_c}) = 10^{\left(\begin{array}{l} -0.1\times\left(10\, n_{f_c}\log_{10}(d_{\text{ter},\,f_c}) + X_{d_{\text{ter}}}^{f_c} + \gamma_{d_{\text{ter}}}^{f_c}\right) \\ +0.1\times\left(10\, n_{f_c}\log_{10}(d_{\min}) + X_{d_{\min}}^{f_c} + \gamma_{d_{\min}}^{f_c}\right)\end{array}\right)}$$

$$\alpha_{\text{ter}}^{\text{nor}}(d_{\text{ter},\,f_c}) = 10^{\left(\begin{array}{l} -n_{f_c}\log_{10}(d_{\text{ter},\,f_c}) \\ +n_{f_c}\log_{10}(d_{\min})\end{array}\right)}\, 10^{\left(\begin{array}{l} -0.1\times\left(X_{d_{\text{ter}}}^{f_c} + \gamma_{d_{\text{ter}}}^{f_c}\right) \\ +0.1\times\left(X_{d_{\min}}^{f_c} + \gamma_{d_{\min}}^{f_c}\right)\end{array}\right)}$$

$$\alpha_{\text{tra}}^{\text{nor}}(d_{\text{ter},\,f_c}) = 10^{\log_{10}\left(\frac{d_{\min}}{d_{\text{ter},\,f_c}}\right)^{n_{f_c}}}\, 10^{\left(\begin{array}{l} -0.1\times\left(X_{d_{\text{ter}}}^{f_c} + \gamma_{d_{\text{ter}}}^{f_c}\right) \\ +0.1\times\left(X_{d_{\min}}^{f_c} + \gamma_{d_{\min}}^{f_c}\right)\end{array}\right)}$$

$$\alpha_{\text{ter}}^{\text{nor}}(d_{\text{ter},\,f_c}) = \left[10^{\left(\frac{\left(X_{d_{\min}}^{f_c} - X_{d_{\text{ter}}}^{f_c} + \gamma_{d_{\min}}^{f_c} - \gamma_{d_{\text{ter}}}^{f_c}\right)}{10}\right)}\right] \times \left(\frac{d_{\min}}{d_{\text{ter},\,f_c}}\right)^{n_{f_c}}. \tag{10}$$

If the shadowing effect is considered the same for all links indoors, eqn. (10) simplifies to the following

$$\alpha_{\text{ter}}^{\text{nor}}\left(d_{\text{ter},\ f_c}\right) \quad \cong \left[10^{\left(\left(\gamma_{d_{\min}}^{f_c} - \gamma_{d_{\text{ter}}}^{f_c}\right)/10\right)}\right] \times \left(\frac{d_{\min}}{d_{\text{ter},\ f_c}}\right)^{n_{f_c}}. \quad (11)$$

The above equation can be further simplified to the following if the floor penetration loss is assumed to be the same for all inter-floor co-channel interferer links

$$\alpha_{\text{ter}}^{\text{nor}}\left(d_{\text{ter},\ f_c}\right) \quad \cong \left(\frac{d_{\min}}{d_{\text{ter},\ f_c}}\right)^{n_{f_c}}. \quad (12)$$

Remark 3 (Partition Loss and Shadowing Effect): Modeling internal wall or partition loss can be overcome by considering more shadowing effects on a link. Such practice can be seen in the existing literature, including the simplified 3$^{\text{rd}}$ Generation Partnership Project (3GPP) path loss model for small cells in indoor environments for the 4G LTE standard, e.g., [62], [63], [64], [65], [66], which considers the shadowing effect of 10 dB standard deviation (STD) for the desired link and 8 dB STD for the interferer link to a SCUE in contrast to a typical STD of 4 dB considered by other path loss models. However, the existence of LOS components in high-frequency mmWave and THz bands is relatively higher than that in low-frequency microwave bands in indoor environments. Further, over a short distance, indoor channels are grossly similar due to incomparable unchanged structures within a local area [67]. Since all apartments in each multi-floor building are assumed to have a similar structure, we consider a similar shadowing effect on each indoor link.

Since we consider the normalized value of the CCI power of any co-channel small cell at any distance from the serving SCUE with respect to the interference power of the co-channel small cell at the nearest minimum distance, the common shadow fading effect components of the links existing between the serving SCUE and any co-channel small cell and between the serving SCUE and its nearest co-channel small cell cancel one another. Hence, considering the shadow fading effect and the internal wall or partition losses in the proposed model is unnecessary, and simplified expressions for both intra-floor (such as in (7)) and inter-floor (such as in (12)) interferences can be applied with reasonable accuracy.

Remark 4 (Effect of Molecular Absorption): The molecular absorption effect occurs concurrently with the free-space propagation of a THz electromagnetic wave. While experiencing free-space path loss, THz electromagnetic waves may excite or resonate with certain categories of molecules inside the non-vacuum medium [68]. A molecule can transit from a high to a low energy level by emitting photons, whereas from a low to a high energy level by absorbing external photons. Absorption of photons causes attenuation, whereas emission of photons brings additional noise to the THz electromagnetic wave [68]. Note that the molecular absorption effect is considerably weak in microwave and mmWave bands causing it to be considered one of the key features of the THz spectrum.

Molecular absorption loss is modeled by the sum of the absorbed power by molecules along the propagation path of the electromagnetic wave, which can be found by taking the product of molecular absorption coefficient k (dB/km) and the propagation distance d (km). The molecular absorption coefficient is triple selective, including frequency, distance, and environmental parameters (e.g., pressure, temperature, and the composition of the medium). More specifically, from the frequency selective perspective, numerous molecular absorption peaks are formed in THz bands at resonant frequencies, and spectral windows between these absorption peaks of multi-GHz bandwidths are recommended for THz wireless transmissions to avoid facing molecular absorption loss [69]. From the distance dependence perspective, though the molecular absorption loss first appears negligible, the loss increases rapidly with increasing propagation distance leading to limiting the THz coverage. As proposed in [70], this can be overcome by employing distance-adaptive communication that adjusts transmission frequency dynamically with distance to avoid distance-dependent absorption peaks. Finally, from the environmental dependence perspective, because of its close dependency on the water vapor concentration along the THz propagation path, the molecular absorption effect varies considerably with the variation in the THz communication environment.

On the contrary, in indoor THz communications, the molecular absorption effect is independent of distance adaptiveness, environment dependency, and location dependency [68]. Particularly, indoor environments are insusceptible to weather conditions leading to insignificant changes in water vapor concentration, which dominates the molecular absorption most among all common air components [71], on rainy or snowy days. Further, environmental parameters such as pressure, temperature, and moisture in indoor environments are relatively stable leading to a favorable condition for THz communications. Furthermore, the maximum distance for indoor THz communications is limited by the dimensions of the indoor environment. All these above indoor characteristics limit the indoor molecular absorption coefficient allowing the design of an indoor THz system not to consider distance adaptiveness and environment dependency of the molecular absorption effect. In addition, because of insignificant variation among various geographical locations in indoor environments, it may be unnecessary to consider the location dependency of the molecular absorption effect [68]. Hence, based on the above discussion on the indoor molecular absorption effect, we assume no molecular absorption effect when modeling indoor THz communications.

Remark 5 (Effect of Link Blockages): In indoor environments, high-frequency mmWave and THz directional links are affected considerably by stationary and moving blockages, including indoor walls, furniture, and human bodies [72]. These blockages may cause sudden link failures affecting the reliability and latency requirements of a mobile network [73]. Recall that, to estimate the path loss, we consider employing the directional LOS 1 m CI free space reference distance model, which incorporates the variation in the large-scale shadow fading over different mmWave and THz frequency bands as given in Table 2. Further, in modeling CCI given by (5) and (8), we consider both the partition loss and shadowing effect.

Partition loss incorporates the internal wall blockage effect between a SCUE and a co-channel interferer. The shadowing effect incorporates other miscellaneous indoor blockage effects such as furniture and human bodies mentioned above. This is because, blockage effects are traditionally incorporated into the large-scale shadowing model when operating at mmWave and THz frequencies (due to the small wavelength), together with reflection, scattering, and diffraction [74]. This implies that, intuitively, indoor blockage effects (including indoor walls, furniture, and human bodies) on mmWave and THz bands are considered in the proposed model.

C. 3D CLUSTERING OF APARTMENTS

Since co-channel interferers exist at both intra-floor and inter-floor levels for a serving SCUE, the overall interference at an SCUE is given by the sum of the intra-floor interference $\alpha_{\text{tra}}^{\text{tot}}$ and inter-floor interference $\alpha_{\text{ter}}^{\text{tot}}$ as given below

$$\alpha_{\text{tot},3\text{D}}^{\text{nor}} = \alpha_{\text{tra}}^{\text{tot}} + \alpha_{\text{ter}}^{\text{tot}}. \tag{13}$$

Note that $\alpha_{\text{tra}}^{\text{tot}} = \sum_{i=1}^{i_{\max}} \alpha_{\text{tra},i}^{\text{nor}}$ and $\alpha_{\text{ter}}^{\text{tot}} = \sum_{j=1}^{j_{\max}} \alpha_{\text{ter},\ j}^{\text{nor}}$, where $i \in \{0, 1, 2, \ldots, i_{\max}\}$ and $j \in \{0, 1, \ldots, j_{\max}\}$.

Let $\alpha_{\text{tra}}^{\text{opt}}$ and $\alpha_{\text{ter}}^{\text{opt}}$ be the maximum allowable interference power from all the intra-floor co-channel interferers and inter-floor co-channel interferers, respectively, at the serving SCUE such that the following holds

$$\alpha_{\text{tra}}^{\text{tot}} \leq \alpha_{\text{tra}}^{\text{opt}} \tag{14}$$

$$\text{and} \quad \alpha_{\text{ter}}^{\text{tot}} \leq \alpha_{\text{ter}}^{\text{opt}}. \tag{15}$$

Then from (13), we can write the following

$$\alpha_{\text{tot},3\text{D}}^{\text{nor}} \leq \alpha_{\text{tra}}^{\text{opt}} + \alpha_{\text{ter}}^{\text{opt}} \tag{16}$$

$$\text{and} \quad \alpha_{\text{tra}}^{\text{tot}} + \alpha_{\text{ter}}^{\text{tot}} \leq \alpha_{\text{tra}}^{\text{opt}} + \alpha_{\text{ter}}^{\text{opt}}. \tag{17}$$

Note that, $\alpha_{\text{tra}}^{\text{opt}}$ and $\alpha_{\text{ter}}^{\text{opt}}$ aggregately define the quality of the received signal at a serving SCUE set usually by a mobile network operator (MNO).

Our objective is to maximize the capacity of in-building SCBSs. Using Shannon's capacity formula, if we allow to increase $(\alpha_{\text{tra}}^{\text{tot}} + \alpha_{\text{ter}}^{\text{tot}})$, the link quality and hence the link capacity at a serving SCUE *degrades* logarithmically. However,$(\alpha_{\text{tra}}^{\text{tot}} + \alpha_{\text{ter}}^{\text{tot}})$ is directly affected by the distance between a serving SCUE and co-channel interferers at both intra-and inter-floor levels. An increase in $(\alpha_{\text{tra}}^{\text{tot}} + \alpha_{\text{ter}}^{\text{tot}})$ means a decrease in distance from co-channel interferers to a serving SCUE, which in turn minimizes the number of apartments (i.e., the size) of a 3D cluster and maximizes the spectrum reuse factor and hence the capacity in a multi-floor building. Hence, a trade-off between the link quality at a serving SCUE and the spectrum reuse factor is required when maximizing the capacity of SCBSs in a building.

More specifically, to maximize the achievable capacity, we need to select a value of $(\alpha_{\text{tra}}^{\text{tot}} + \alpha_{\text{ter}}^{\text{tot}})$ that can minimize distance and hence the size of a 3D cluster in a building, subject to adhering to the link quality of SCBSs. We term this problem for capacity maximization an *indirect* optimization problem since our objective is to maximize the capacity of in-building SCBSs, not by directly increasing the available spectrum bandwidth of an MNO, but by indirectly reusing more of the MNO's spectrum in SCBSs. Hence, an optimal size of a 3D cluster corresponds to minimizing the 3D cluster size to maximize the spectrum reuse factor and hence the capacity subject to satisfying conditions (13)–(17), and can be found by solving the following problem.

$$\begin{aligned} &\text{minimize} \quad \delta_{3\text{D},\ f_c} \\ &\text{subject to} \quad \text{(a)} \quad \alpha_{\text{tot},3\text{D}}^{\text{nor}} = \alpha_{\text{tra}}^{\text{tot}} + \alpha_{\text{ter}}^{\text{tot}} \\ &\qquad\qquad\quad \text{(b)} \quad \alpha_{\text{tra}}^{\text{tot}} \leq \alpha_{\text{tra}}^{\text{opt}} \\ &\qquad\qquad\quad \text{(c)} \quad \alpha_{\text{ter}}^{\text{tot}} \leq \alpha_{\text{ter}}^{\text{opt}} \\ &\qquad\qquad\quad \text{(d)} \quad \alpha_{\text{tra}}^{\text{tot}} + \alpha_{\text{ter}}^{\text{tot}} \leq \alpha_{\text{tra}}^{\text{opt}} + \alpha_{\text{ter}}^{\text{opt}} \\ &\qquad\qquad\quad \text{(e)} \quad P_{\text{SCBS},\ f_c} \leq P_{\text{SCBS},\ f_c,max}. \end{aligned} \tag{18}$$

where $P_{\text{SCBS},\ f_c,max}$ represents the maximum transmit power of an SCBS operating at f_c.

We consider estimating the total CCI at the intra-floor level and inter-floor at a serving SCUE separately, and the sum of CCI at both levels gives the total interference at an SCUE in the 3D in-building scenario (13). Because (14) and (15) hold, we can define the maximum allowable interference at the intra-floor level $\alpha_{\text{tra}}^{\text{opt}}$ and inter-floor level $\alpha_{\text{ter}}^{\text{opt}}$ independently. However, using (7) and (12), $\alpha_{\text{tra}}^{\text{opt}}$ and $\alpha_{\text{ter}}^{\text{opt}}$ are inversely related to the distance between co-channel base stations at intra-floor and inter-floor levels, respectively. Note that a serving SCBS that serves a serving SCUE is also a co-channel SCBS since they operate at the same frequency.

So, an optimal minimum distance between co-channel SCBSs at both intra-and inter-floor levels is estimated by separating the above minimization problem in (18) into two sub-problems below.

Sub-problem 1:

$$\begin{aligned} &\text{minimize} \quad d_{\text{tra},f_c} \\ &\text{subject to} \quad \text{(a)} \quad \alpha_{\text{tra}}^{\text{tot}} \leq \alpha_{\text{tra}}^{\text{opt}} \\ &\qquad\qquad\quad \text{(b)} \quad P_{\text{SCBS},\ f_c} \leq P_{\text{SCBS},\ f_c,\max}. \end{aligned}$$

Sub-problem 2:

$$\begin{aligned} &\text{minimize} \quad d_{\text{ter},\ f_c} \\ &\text{subject to} \quad \text{(a)} \quad \alpha_{\text{ter}}^{\text{tot}} \leq \alpha_{\text{ter}}^{\text{opt}} \\ &\qquad\qquad\quad \text{(b)} \quad P_{\text{SCBS},\ f_c} \leq P_{\text{SCBS},\ f_c,\max}. \end{aligned}$$

Solutions to sub-problem 1 and sub-problem 2 give an optimal minimum distance between intra-floor co-channel SCBSs of ${d_{\text{tra},\ f_c}}^*$ and inter-floor co-channel SCBSs of ${d_{\text{ter},\ f_c}}^*$, respectively. These optimal distances in turn give an optimal minimum size for a 3D cluster ${\delta_{\text{3D},\ f_c}}^*$ that maximizes the capacity while satisfying the CCI constraints separately at both intra-floor (i.e., 18(b)) and inter-floor levels (i.e., 18(c)).

D. MINIMUM DISTANCE ESTIMATION

1) INTRA-FLOOR LEVEL

Considering the worst-case scenario, let $\varepsilon_{\text{tra,max}}$ be the maximum number of intra-floor co-channel interferers in the first tier for a serving SCUE. The aggregate intra-floor CCI experienced by a serving SCUE at $f_c$is given by

$$\alpha_{\text{tra}}^{\text{tot}} = \varepsilon_{\text{tra,max}} \times \left[10^{\left(\left(X_{d_{\min}}^{f_c} - X_{d_{\text{tra}}}^{f_c} + \beta_{d_{\min}}^{f_c} - \beta_{d_{\text{tra}}}^{f_c}\right)/10\right)}\right] \times \left(\frac{d_{\min}}{d_{\text{tra},\ f_c}}\right)^{n_{f_c}}. \tag{19}$$

Note that, for square-grid apartments, the number of intra-floor co-channel interferers in the first tier of co-channel SCBSs, $\varepsilon_{\text{tra,max}} = 8$ for a serving SCUE such that the constraint (a) in sub-problem 1 (i.e., $\alpha_{\text{tra}}^{\text{tot}} \leq \alpha_{\text{tra}}^{\text{opt}}$) can be satisfied when $d_{\text{tra},\ f_c} = {d_{\text{tra},\ f_c}}^*$. Hence, using (19), we can write the following

$$\varepsilon_{\text{tra,max}} \times \left[10^{\left(\left(X_{d_{\min}}^{f_c} - X_{d_{\text{tra}}}^{f_c} + \beta_{d_{\min}}^{f_c} - \beta_{d_{\text{tra}}}^{f_c}\right)/10\right)}\right] \times \left(\frac{d_{\min}}{{d_{\text{tra},\ f_c}}^*}\right)^{n_{f_c}} \leq \alpha_{\text{tra}}^{\text{opt}}. \tag{20}$$

So, from (20), the expression for the minimum distance between intra-floor co-channel small cells at f_c can be expressed as follows

$${d_{\text{tra},\ f_c}}^* = d_{\min} \times \left(10^{\left(\left(X_{d_{\min}}^{f_c} - X_{d_{\text{tra}}}^{f_c} + \beta_{d_{\min}}^{f_c} - \beta_{d_{\text{tra}}}^{f_c}\right)/10\right)} \left(\frac{\varepsilon_{\text{tra,max}}}{\alpha_{\text{tra}}^{\text{opt}}}\right)\right)^{n_{f_c}^{-1}}. \tag{21}$$

2) INTER-FLOOR LEVEL

Let $\varepsilon_{\text{ter,max}}$ be the maximum number of inter-floor co-channel interferers in the first tier for a serving SCUE such that, following (19), the aggregate inter-floor CCI experienced by a serving SCUE at f_c is given by

$$\alpha_{\text{ter}}^{\text{tot}} = \varepsilon_{\text{ter,max}} \times \left[10^{\left(\left(X_{d_{\min}}^{f_c} - X_{d_{\text{ter}}}^{f_c} + \gamma_{d_{\min}}^{f_c} - \gamma_{d_{\text{ter}}}^{f_c}\right)/10\right)}\right] \times \left(\frac{d_{\min}}{d_{\text{ter},\ \text{f}_\text{c}}}\right)^{n_{f_c}}. \tag{22}$$

The value of $\varepsilon_{\text{ter,max}}$ depends on the geometry of the building. More specifically, co-channel interferers may exist on the top and bottom floors of the serving SCUE's floor. Considering the first-tier inter-floor interferers, $\varepsilon_{\text{ter,max}} = 2$ when interferers exist on both the top and bottom floors (i.e., double-sided CCI). However, $\varepsilon_{\text{ter,max}} = 1$ when interferers exist on either the top or the bottom floor (i.e., single-sided CCI). Like intra-floor interferers, the constraint (a) in the sub-problem 2 (i.e., $\alpha_{\text{ter}}^{\text{tot}} \leq \alpha_{\text{ter}}^{\text{opt}}$) can be satisfied when $d_{\text{ter},\ f_c} = {d_{\text{ter},\ f_c}}^*$. Hence, using (22), the following holds

$$\varepsilon_{\text{ter,max}} \times \left[10^{\left(\left(X_{d_{\min}}^{f_c} - X_{d_{\text{ter}}}^{f_c} + \gamma_{d_{\min}}^{f_c} - \gamma_{d_{\text{ter}}}^{f_c}\right)/10\right)}\right] \times \left(\frac{d_{\min}}{{d_{\text{ter},\ f_c}}^*}\right)^{n_{f_c}} \leq \alpha_{\text{ter}}^{\text{opt}}. \tag{23}$$

So, from (23), we can find the minimum distance between inter-floor co-channel small cells at f_c as follows

$${d_{\text{ter},\ f_c}}^* \geq d_{\min} \times \left(10^{\left(\left(X_{d_{\min}}^{f_c} - X_{d_{\text{ter}}}^{f_c} + \gamma_{d_{\min}}^{f_c} - \gamma_{d_{\text{ter}}}^{f_c}\right)/10\right)} \times \left(\frac{\varepsilon_{\text{ter,max}}}{\alpha_{\text{ter}}^{\text{opt}}}\right)\right)^{n_{f_c}^{-1}}. \tag{24}$$

E. SPECTRUM REUSE FACTOR

Let $\tau_{\text{tra},\ f_c}$ be the maximum number of tiers of apartments (Fig. 1(b)) in the RoE to satisfy ${d_{\text{tra},\ f_c}}^*$. We can then find the size of the 2D intra-floor cluster of apartments below

$$\varepsilon_{\text{tra},\ f_c} = 1 + \sum_{\upsilon=1}^{\tau_{\text{tra},\ f_c}} (8 + ((\upsilon - 1) \times 8)). \tag{25}$$

The value of $\tau_{\text{tra},\ f_c}$ can be found as follows

$$\tau_{\text{tra},\ f_c} = \text{ceil}\left(\frac{d_{\text{tra},\ f_c}^*}{a}\right). \tag{26}$$

where $a = 10$ m represents the length of each side of a square apartment. Similar to the 2D intra-floor level, we can find the number of apartments in the third dimension within the 3D RoE at the inter-floor level satisfying ${d_{\text{ter},\ f_c}}^*$ at f_c as follows

$$\varepsilon_{\text{ter},\ f_c} = \varepsilon_{\text{ter,max}} \times \text{ceil}\ \left(d_{\text{ter},\ f_c}^* / d_{\text{floor}}\right), \tag{27}$$

where d_{floor} represents the floor height of a building. $\varepsilon_{\text{ter,max}} = 1$ for single-sided CCI and $\varepsilon_{\text{ter,max}} = 2$ for double-sided CCI at the inter-floor level.

Hence, an *optimal size* of a 3D cluster satisfying the constraints in (5) can be found as follows

$${\delta_{\text{3D},\ f_c}}^* = \left(\varepsilon_{\text{tra},\ f_c} \times \varepsilon_{\text{ter},\ f_c}\right). \tag{28}$$

Let $\varepsilon_{\text{RF},\ f_c}$ be the spectrum reuse factor of a building of $S_{\text{APT}}^{\text{buil}}$ apartments, which is defined as the number of times the same spectrum can be reused in small cells of these apartments at f_c and is given by

$$\varepsilon_{\text{RF},\ f_c} = \frac{S_{\text{APT}}^{\text{buil}}}{{\delta_{\text{3D},\ f_c}}^*} \tag{29}$$

$$\varepsilon_{\text{RF},\ f_c} = \frac{S_{\text{APT}}^{\text{buil}}}{\left(\varepsilon_{\text{tra},\ f_c} \times \varepsilon_{\text{ter},\ f_c}\right)}. \tag{30}$$

In estimating the number of SCBSs in a 3D cluster and hence in a building, it is to be noted that, in practice, the number of SCBSs per 3D cluster can vary from one cluster to another in a building. Hence, we consider the following *two cases* based on whether or not an apartment may have an SCBS installed.

1) CASE 1 (STATIC PLACEMENT OF SCBSS PER APARTMENT): ONE SCBS PER APARTMENT

Let cl_{f_c} denote any 3D cluster with SCBSs operating at f_c in a building such that $cl_{f_c} = \{1, 2, \ldots, \varepsilon_{RF,\ f_c}\}$. Assume that each apartment in a building is equipped with *exactly* one SCBS such that the number of SCBSs in cl_{f_c} is the same as the number of apartments in cl_{f_c} and hence is given by

$$S^{3D,cl_{f_c}}_{SCBS,\ f_c} = S^{3D}_{SCBS,m,\ f_c} = \delta_{3D,\ f_c}{}^*,$$

where $S^{3D}_{SCBS,m,\ f_c}$ defines the maximum number of SCBSs per 3D cluster, which is also the same for all 3D clusters in a building at f_c. Likewise, the number of apartments in a building is given by $S^{buil}_{APT} = S^{buil}_{SCBS,f_c}$ where S^{buil}_{SCBS,f_c} denotes the number of SCBSs at f_c in a building.

We can now find the spectrum reuse factor at f_c in terms of the number of SCBSs as follows

$$\varepsilon_{RF,\ f_c} = \frac{S^{buil}_{SCBS,f_c}}{S^{3D}_{SCBS,m,\ f_c}}. \tag{31}$$

2) CASE 2 (RANDOM PLACEMENT OF SCBSS PER APARTMENT): A MAXIMUM OF ONE SCBS PER APARTMENT

Now, if we assume that each apartment in a building is equipped with a *maximum* of one SCBS, then the number of SCBSs in cl_{f_c}, $S^{3D,cl_{f_c}}_{SCBS,\ f_c}$, and in a building, $S^{buil}_{SCBS,\ f_c}$, is given by

$$S^{3D,cl_{f_c}}_{SCBS,\ f_c} = \sum_{s=1}^{s_m} 1_{q_s}(\kappa_s)\kappa_s$$

$$\text{and} \quad S^{buil}_{SCBS,\ f_c} = \sum_{cl_{f_c}=1}^{cl_{f_c,m}} S^{3D,cl_{f_c}}_{SCBS,\ f_c},$$

where $q_s \in \{\kappa_1, \kappa_2, \ldots, \kappa_{s_m}\}$ and

$$1(\cdot) = \begin{cases} 1, \text{ if } \kappa_s \text{ exists in the set } q_s \text{ for any } s \\ 0, \text{ otherwise} \end{cases}$$

For simplicity, we consider the same number of SCBSs withincl_{f_c} in a building, i.e., $\forall cl_{f_c}$, $S^{3D,cl_{f_c}}_{SCBS,\ f_c} = S^{3D}_{SCBS,\ f_c}$. This, however, would not affect considerably the average capacity per 3D cluster. This is because the coverage area of an indoor SCBS is small and the speed of objects, including SCUEs, is low, resulting in less variation in indoor channel characteristics at high frequencies such as mmWave and THz bands.

Nevertheless, the randomness in the number of SCBSs in 3D clusters does not affect the spectrum reuse factor as the spectrum reuse factor is defined by the number of apartments per 3D cluster and hence is given by

$$\varepsilon_{RF,\ f_c} = \frac{S^{buil}_{APT}}{\delta_{3D,\ f_c}{}^*}. \tag{32}$$

From the above analysis, the values of $d^*_{tra,\ f_c}$ and $d^*_{ter,\ f_c}$ from an SCBS located on any floor in a multi-story building define the size of a 3D cluster $\delta_{3D,\ f_c}{}^*$ at f_c,. Because $|\delta_{3D,\ f_c}{}^*|$ changes with a change in f_c, following the above generic model, GSRM, we can find $|\delta_{3D,\ f_c}{}^*|$ and hence, the spectrum reuse factor $\varepsilon_{RF,\ f_c}$ corresponding to any mmWave and THz frequency. Moreover, depending on whether or not an apartment is equipped with an SCBS, the exact number of SCBSs per 3D cluster and hence in a building can be estimated.

IV. MATHEMATICAL ANALYSIS AND PERFORMANCE METRICS ESTIMATION

A. MULTI-TIER NETWORKS MODEL

Let all macrocell user indices be denoted by a set $Y_M = \{1, 2, \ldots, Y\}$. Y_M is partitioned randomly into three disjoint subsets, Y_{MI} for indoor macrocell user indices, Y_P for picocell user indices, and Y_{MO} for outdoor macrocell user indices. The maximum number of active femtocell base stations in cl_{f_c} in a building is given by $S^{3D,cl_{f_c}}_{SCBS,\ f_c} = S^{cl_{f_c}}_{f_c}$ such that $s \in \{1, 2, \ldots, S^{cl_{f_c}}_{f_c}\}$. Denote L as the number of buildings over the coverage of a macrocell such that $l = \{1, 2, \ldots, L\}$. Let M_{f_c} denote the number of RBs in the bandwidth of f_c such that $m_{f_c} \in M_{f_c} = \{M_{28}, M_{142}, M_{220}, M_{300}\}$. For simplicity, we assume each SCBS is enabled with the same multi-band mmWave and THz frequency of F_c.

Let P_{f_c} denotes the transmission power of an SCBS when operating at f_c. The transmission power of an MCBS and a PCBS, respectively, are denoted by P_{MC} and P_{PC}. Let $S_M$and S_P be the number of MCBSs and PCBSs, respectively. Note that an RB is equal to 180 kHz, and both the macrocell and all picocells run only on the 2 GHz microwave spectrum. Let $\boldsymbol{T}$ denote simulation run time with the maximum time of Q (in time steps each lasting 1 ms) such that $\boldsymbol{T} = \{1, 2, 3, \ldots, Q\}$.

B. PERFORMANCE METRICS ESTIMATION

Using Shannon's capacity formula, a link throughput at RB $= i$ in TTI $=$ t in bps per Hz is given by

$$\sigma_{t,i}(\rho_{t,i}) = \left\{ \begin{array}{cc} 0, & \rho_{t,i} < -10 \text{ dB} \\ \beta \log_2\left(1 + 10^{\left(\frac{\rho_{t,i}(\text{dB})}{10}\right)}\right) & -10 \text{ dB} \leq \rho_{t,i} \leq 22 \text{ dB} \\ 4.4, & \rho_{t,i} > 22 \text{ dB} \end{array} \right\}, \tag{33}$$

where $\rho_{t,i}$ represents the received signal-to-interference-plus-noise ratio (SINR) at RB $= i$ in TTI $=$ t for a UE in the downlink. β represents the implementation loss factor.

1) MACROCELL NETWORKS

Recall that all macrocell UEs are served at the 2 GHz microwave spectrum. Hence, the aggregate capacity of the macrocell UEs is given by

$$\sigma^{macro}_{2GHz} = \sum_{t \in \boldsymbol{T}} \sum_{i=1}^{M_2} \sigma_{t,i}(\rho_{t,i}), \tag{34}$$

where σ and ρ denote, respectively, throughput and SINR responses of macrocell UEs over M_2 RBs in $t \in \boldsymbol{T}$.

2) SMALL CELL NETWORKS

Because each SCBS is enabled with $|F_c|$ frequencies, the capacity served by any SCBSs incl_{f_c} is given by

$$\sigma^{\text{scbs}}_{s,f_c,t,i} = \sum_{t\in \boldsymbol{T}} \sum_{i=1}^{M_{f_c}} \sigma_{s,f_c,t,i}\big(\rho_{s,f_c,t,i}\big). \tag{35}$$

Hence, the capacity served by allF_c operated by $|F_c|$ transceivers of an SCBS s in $cl_{f_c}$is given by

$$\sigma^{\text{scbs}}_{s,F_c,t,i} = \sum_{f_c\in F_c} \sum_{t\in \boldsymbol{T}} \sum_{i=1}^{M_{f_c}} \sigma_{s,f_c,t,i}\big(\rho_{s,f_c,t,i}\big). \tag{36}$$

Assume that all SCBSs within each 3D cluster serve simultaneously in $t \in \boldsymbol{T}$ at all F_c. Then, the total capacity served by all SCBSs in $cl_{f_c}$is given by the following

$$\sigma^{\text{scbs}}_{cl_{f_c},S^{cl_{f_c}}_{f_c},F_c,t,i} = \sum_{s\in S^{cl_{f_c}}_{f_c}} \sum_{f_c\in F_c} \sum_{t\in \boldsymbol{T}} \sum_{i=1}^{M_{f_c}} \sigma_{s,f_c,t,i}\big(\rho_{s,f_c,t,i}\big). \tag{37}$$

Similarly, the total capacity served by all 3D clusters in any building l is given by the following

$$\sigma^{\text{scbs}}_{l,\varepsilon_{\text{RF},f_c},S^{cl_{f_c}}_{f_c},F_c,t,i} = \sum_{cl_{f_c}\in\varepsilon_{\text{RF},f_c}} \sum_{s\in S^{cl_{f_c}}_{f_c}} \sum_{f_c\in F_c} \sum_{t\in \boldsymbol{T}} \sum_{i=1}^{M_{f_c}} \sigma_{cl_{f_c},s,f_c,t,i}\big(\rho_{cl_{f_c},s,f_c,t,i}\big). \tag{38}$$

For simplicity, we consider a similar structure for each building, including the same number of SCBSs per floor and the number of floors per building. Moreover, because of the short distance between an SCBS and its serving UE and the low transmission power of an SCBS, indoor signal propagation characteristics remain similar across several buildings located over the macrocell coverage.

- *Only In-building Small Cell Networks:* The average aggregate capacity for L number of buildings of SCBSs can be found by linear approximation and is given by

$$\sigma^{\text{scbs,CA}}_{L,\varepsilon_{\text{RF},f_c},S^{cl_{f_c}}_{f_c},F_c,t,i} = \sum_{l\in L} \sum_{cl_{f_c}\in\varepsilon_{\text{RF},f_c}} \sum_{s\in S^{cl_{f_c}}_{f_c}} \sum_{f_c\in F_c} \sum_{t\in \boldsymbol{T}} \sum_{i=1}^{M_{f_c}} \sigma_{l,cl_{f_c},s,f_c,t,i}\big(\rho_{l,cl_{f_c},s,f_c,t,i}\big). \tag{39}$$

Assume that each SCBS is allocated to the same amount of RBs of each frequency band. The SE for L buildings is then given by

$$\sigma^{\text{scbs,SE}}_{L,\varepsilon_{\text{RF},f_c},S^{cl_{f_c}}_{f_c},F_c,t,i} = \frac{\sigma^{\text{scbs,CA}}_{L,\varepsilon_{\text{RF},f_c},S^{cl_{f_c}}_{f_c},F_c,t,i}}{\Big(S^{cl_{f_c}}_{f_c} \times \sum_{f_c\in F_c} M_{f_c}\Big) \times Q}. \tag{40}$$

Likewise, the EE for L buildings is given by

$$\sigma^{\text{scbs,EE}}_{L,\varepsilon_{\text{RF},f_c},S^{cl_{f_c}}_{f_c},F_c,t,i} = \left(\sum_{l\in L} \sum_{cl_{f_c}\in\varepsilon_{\text{RF},f_c}} \sum_{s\in S^{cl_{f_c}}_{f_c}} \sum_{f_c\in F_c} P_{l,cl_{f_c},s,f_c}\right) \Bigg/ \left(\frac{\sigma^{\text{scbs,CA}}_{L,\varepsilon_{\text{RF},f_c},S^{cl_{f_c}}_{f_c},F_c,t,i}}{Q}\right). \tag{41}$$

- *Overall Multi-tier System:* The overall system-level average aggregate capacity for the multi-tier system can be found by considering the contributions of all the cells in the system (i.e., the macrocell, picocells, and in-building small cells) as follows

$$\sigma^{\text{overall, CA}}_{L,\varepsilon_{\text{RF},f_c},S^{cl_{f_c}}_{f_c},F_c,t,i} = \sigma^{\text{macro}}_{2\text{ GHz}} + \sigma^{\text{scbs,CA}}_{L,\varepsilon_{\text{RF},f_c},S^{cl_{f_c}}_{f_c},F_c,t,i}. \tag{42}$$

The overall system-level SE for the multi-tier system is then given by

$$\sigma^{\text{overall, SE}}_{L,\varepsilon_{\text{RF},f_c},S^{cl_{f_c}}_{f_c},F_c,t,i} = \frac{\sigma^{\text{overall, CA}}_{L,\varepsilon_{\text{RF},f_c},S^{\text{cl}}_{f_c},F_c,t,i}}{\Big(M_2 + \Big(S^{cl_{f_c}}_{f_c} \times \sum_{f_c\in F_c} M_{f_c}\Big)\Big) \times Q}. \tag{43}$$

Similarly, the overall system-level EE for the multi-tier system is then given by

$$\sigma^{\text{overall, EE}}_{L,\varepsilon_{\text{RF},f_c},S^{cl_{f_c}}_{f_c},F_c,t,i} = \left(\begin{array}{c}(S_M \times P_{\text{MC}}) + (S_P \times P_{\text{PC}}) + \\ \Big(\sum_{l\in L} \sum_{cl_{f_c}\in\varepsilon_{\text{RF},f_c}} \sum_{s\in S^{cl_{f_c}}_{f_c}} \sum_{f_c\in F_c} P_{l,cl_{f_c},s,f_c}\Big)\end{array}\right) \Bigg/ \left(\frac{\sigma^{\text{overall,CA}}_{L,\varepsilon_{\text{RF},f_c},S^{cl_{f_c}}_{f_c},F_c,t,i}}{Q}\right). \tag{44}$$

V. ALGORITHM AND SIMULATION ASSUMPTIONS AND PARAMETERS

A. PROPOSED ALGORITHM

In Algorithm 1, we propose an algorithm following a step-wise approach to execute the GSRM and evaluate its performance in a multi-tier system. Key parameters, including intra-floor and inter-floor CCIs, corresponding minimum distances between small cells, a 3D cluster size, and spectrum reuse factor per building for each f_c are estimated to evaluate SE and EE performances of the GSRM under both scenarios. Finally, the SE and EE performances of the GSRM are compared against the expected SE and EE performances of the future 6G mobile system.

B. SIMULATION ASSUMPTIONS AND PARAMETERS

Default simulation parameters and assumptions, which are used for the system-level evaluation of a multi-tier system are given in Table 3. Recall that the macrocell and picocells operate at the 2 GHz frequency, which is not reused in small cells. Because analyzing the full spectrum of mmWave and THz (e.g., from 10 GHz to 300 GHz) frequencies is difficult, we consider sample frequencies of 28 GHz for

Algorithm 1 A Stepwise Approach to Developing the Proposed GSRM and Evaluating Its SE and EE Performances

// start

//parameters and assumptions

Step 01. Define the number of outdoor, indoor, and offloaded macrocell UEs where the macrocell serves all indoor and outdoor macrocell UEs, and picocells serve offloaded macrocell UEs.

Step 02. Define the maximum number of multi-floor buildings L such that $l = \{1, 2, ..., L\}$over a macrocell coverage. Now, count the number of floors and the number of apartments per floor in each building. Assume each apartment is a square and one SCBS per apartment that serves one SCUE at a time.

Step 03. Select the type of mmWave and THz frequency bands and define bandwidth, partition loss, SCBS transmit power, and channel parameters of the CI path loss model (PLE and shadow fading) of each band.

//GSRM modeling

// CCI modeling in SCBSs

Step 04. For any building l, find the closest co-channel interferer distance from a SCUE ($d_{\min}$). Now, estimate each CCI power (normalized to that of the closest interferer at $d_{\min}$) at both intra-floor ($\alpha^{\text{nor}}_{\text{tra},i}$) and inter-floor ($\alpha^{\text{nor}}_{\text{ter},\ j}$) levels at each SCUE in a building for all mmWave and THz frequency bands where$i \in \{0, 1, 2, \ldots, i_{\max}\}$and $j \in \{0, 1, \ldots, j_{\max}\}$.

//Algorithm 1 (continued)

Step 05. Estimate the total CCI power at both intra-floor ($\alpha^{\text{tot}}_{\text{tra}}$) and inter-floor ($\alpha^{\text{tot}}_{\text{ter}}$) levels to compute the overall CCI in 3D ($\alpha^{\text{nor}}_{\text{tot,3D}} = \alpha^{\text{tot}}_{\text{tra}} + \alpha^{\text{tot}}_{\text{ter}}$), and define the maximum allowable CCI power at both intra-floor ($\alpha^{\text{opt}}_{\text{tra}}$) and inter-floor ($\alpha^{\text{opt}}_{\text{ter}}$) levels at each SCUE in a building for all frequency bands such that $\alpha^{\text{tot}}_{\text{tra}} \leq \alpha^{\text{opt}}_{\text{tra}}$, $\alpha^{\text{tot}}_{\text{ter}} \leq \alpha^{\text{opt}}_{\text{ter}}$, and $\alpha^{\text{nor}}_{\text{tot,3D}} \leq \alpha^{\text{opt}}_{\text{tra}} + \alpha^{\text{opt}}_{\text{ter}}$hold.

// minimum distance and 3D clustering

Step 06. Now, estimate the minimum distance between co-channel small cells at both intra-floor ($d_{\text{tra}}{}^*$) and inter-floor ($d_{\text{ter}}{}^*$) levels subject to satisfying $\alpha^{\text{tot}}_{\text{tra}} \leq \alpha^{\text{opt}}_{\text{tra}}$ and$\alpha^{\text{tot}}_{\text{ter}} \leq \alpha^{\text{opt}}_{\text{ter}}$, respectively, for all bands.

Step 07. Find the number of apartments at both intra-floor (ε_{tra}) and inter-floor (ε_{ter}) levels corresponding to $d_{\text{tra}}{}^*$ and $d_{\text{ter}}{}^*$, respectively, which gives the optimal size of a 3D cluster $\delta_{3\text{D}}{}^* = (\varepsilon_{\text{tra}} \times \varepsilon_{\text{ter}})$, which is the same in scenario 1 for all bands and can be different in scenario 2 for different bands. now, reuse the bandwidth of each band to SCBSs in each $\delta_{3\text{D}}{}^*$.

// spectrum reuse factor

Step 08. Estimate the spectrum reuse factor in building l of$S^{\text{buil}}_{\text{APT}}$apartments ($\varepsilon_{\text{RF}} = \frac{S^{\text{buil}}_{\text{APT}}}{\delta_{3\text{D}}{}^*}$) for each band under scenario 1 and scenario 2, regardless of the static (case 1) or random (case 2) placement of SCBSs per 3D cluster, and evaluate the average capacity.

Step 09. Repeat Step 01 through Step 08 for all buildings L within the macrocell coverage under scenario 1 and scenario 2.

// performance metrics

Step 10. Evaluate the performance of GSRM in terms of average capacity, SE, and EE for all buildings L in view of only the in-building small cell network as well as the overall multi-tier system under scenario 1 and scenario 2.

Step 11. Also, observe the impact of varying the spectrum reuse factor and the number of buildings on SE and EE performances of GSRM under different scenarios, including the default scenario of no spectrum reuse, scenario 1, and scenario 2.

// Performance comparison

Step 12. Finally, examine the viability of SE and EE performances in Step 10 for a change in the spectrum reuse factor and the number of buildings of the proposed GSRM against the prospective SE and EE performances of the future 6G mobile system.

// End

the spectrum ranging from 1 GHz to 100 GHz, 142 GHz for the spectrum ranging from 101 GHz to 200 GHz, and both 250 GHz and 300 GHz for the spectrum ranging from 201 GHz to 300 GHz. SCBSs are evaluated under two scenarios described earlier. Note that when reusing any RB j to an SCBS s in an apartment, the spectrum resource scheduler needs to identify all apartments that are at least $d_{\text{tra},f_c}{}^*$ distance away at the intra-floor level, and $d_{\text{ter},f_c}{}^*$ distance away at the inter-floor level, from s to reuse RB j to SCBSs of those apartments. This implies that an RB can be reused dynamically per SCBS basis, and an apartment in a building may not be equipped with an SCBS. Numerous assumptions are highlighted with relevant clarification in what follows.

1) ONE SCBS PER APARTMENT

SCBSs such as femtocell base stations are low-power, low-cost base stations, which typically provide coverage of a range of 40 meters [81]. In general, apartments in a building are square or rectangular. Hence, to keep consistent with the practical scenario, we assume each apartment is square, with a side length of 10 meters and a height of 3 meters. An SCBS then needs to provide a maximum coverage of $5\sqrt{2}$meters (which is much smaller than 40 meters) at the worst-case scenario. Hence, considering one SCBS per apartment is sufficient to provide full coverage within a square apartment with a side length of 10 meters.

2) MULTI-TRANSCEIVER ENABLED SCBSS

The number of transceivers, and their operating frequencies, of an SCBS impacts considerably the data rate and capacity it serves. Usually, the link data rate and capacity of an SCBS increase with increasing the number of transceivers and their operating frequencies [82]. This is, particularly, significant when moving toward high frequencies because of the low multipath fading effect and high signal directivity of high frequencies. Such characteristics of signals at high frequencies drive indoor SCBSs to be enabled with multiple transceivers operating at mmWave and THz frequency bands to address the high capacity and data rate demands of next-generation mobile communications. In line with this, we consider that each in-building SCBS is enabled with four transceivers.

3) INTERNAL WALL OR PARTITION LOSS

Internal wall or partition loss varies with the thickness and type of the material used and the antenna polarization at any frequency. Besides, the partition loss is frequency-dependent and usually increases with an increase in frequency. For example, partition loss (in dB) for the clear glass is 1.5 at 28 GHz and 10.22 at 140 GHz [54]. Usually, the partition loss increases with an increase in operating frequency. Because high-frequency signals, such as mmWave and THz, suffer highly from the distance-dependent path loss and lightly from the multipath fading effect, we assume similar channel responses for all co-channel interferers to define the normalized interference, along with considering large-scale shadow fading and no small-scale fading at a serving SCUE.

4) FLOOR PENETRATION LOSS

The floor penetration loss is non-linear and decreases as the number of floors between transceivers increases. For example, at a high frequency such as 28 GHz mmWave, the floor penetration loss (in dB) is about 53, 63, and 67 at the first, second, and third floors, respectively [83]. So, if we even consider only the first floor, a signal can hardly pass through it. Because the floor penetration loss is frequency-dependent and increases with an increase in frequency [83],

the floor penetration loss at any frequency higher than 28 GHz will increase further. Hence, it can be safely assumed that the effect of CCI on adjacent floors at 28 GHz, 142 GHz, 250 GHz, and 300 GHz frequencies is insignificant and can be reused these frequencies to SCBSs on each floor in a multi-story building. So, there is no CCI effect from SCBSs of one floor to SCBSs of adjacent floors at 28 GHz, 142 GHz, 250 GHz, and 300 GHz frequencies.

5) SMALL CELLS OF ADJACENT BUILDINGS

In addition to intra-and inter-floor CCIs, CCIs can be generated when reusing the same frequency to SCBSs of an adjacent building. However, due to the low transmission power of an SCBS, high external wall penetration losses from both buildings, a minimum space requirement between adjacent buildings (i.e., 20 m), and high-frequency mmWave and THz signals, we assume no CCI effect from SCBSs of adjacent buildings even though the same mmWave and THz frequencies are reused to SCBSs of all buildings L over the macrocell coverage.

VI. PERFORMANCE EVALUATION

A. IMPACT OF INTERFERENCE THRESHOLD ON SPECTRUM REUSE FACTOR

We vary the interference thresholds at both intra-floor and inter-floor levels from 0.05 to 0.4 (normalized values) to show how the minimum distance requirements change at both levels to limit the maximum allowable aggregate interference at the SCUE. After carrying out extensive simulations, major observations are discussed in the following.

- With increasing frequency, the required minimum distance decreases. This implies that more spectrum reuse can be made due to high impediment to the interference and penetration and partition losses along with less non-light-of-sight (NLOS) effect. However, note that the observation is based on the path loss exponent only, which can be varied from one frequency band to another with a change in shadow fading effect. In fact, it is not always the case that the path loss exponent follows a uniform pattern. For example, with an increase in frequency, the path loss exponent increases. However, this is always not the case, and since the shadow fading effect also changes nonlinearly, the exact response can be found when we do real-field experiments. Yet, the proposed GSRM gives us some important insights into how carrier frequency affects the resource reuse factor within a building using a simple model.
- From Fig. 4, it can be found that, with increasing interference threshold (i.e., degrading the signal quality) at the SCUE, the minimum distance requirement between co-channel SCBSs decreases meaning that more reuse of the same spectrum can be made in the same building.
- The minimum distance requirement does not change linearly with a change in the interference threshold. Rather, the impact of the interference threshold on the minimum distance requirement is higher for lower values of interference thresholds (i.e., for better signal qualities).
- Likewise, the frequency band significantly impacts the minimum distance requirement (i.e., spectrum reuse factor) at both intra-floor and inter-floor levels for a low interference threshold (e.g., 5% or 0.05) at the serving SCUE.
- Also, the change in minimum distance requirement is less for higher frequency bands and vice versa.

Remark 6 (Minimum Distance Between Co-Channel Interferers): In practice, the actual arrangement of the internal wall or partition loss as well as the floor penetration loss varies from one building to another. In such an unpredictable scenario, defining the exact values of these losses is difficult. That's why, we consider the normalized value of interference in deriving minimum distance between co-channel SCBSs such that these losses can be canceled out of each other for any arbitrary co-channel interferer with respect to the closest co-channel interferer to the SCUE. Note that, the exact value of the minimum distance required at both intra-and inter-floor can be found by carrying out site-specific real-time experiments to measure the accurate inter-floor penetration loss and the intra-floor partition loss along with large-scale fading effect and putting all these values to the expression for a minimum distance at both intra- and inter-floor levels given in (17) and (20), respectively.

B. PATH LOSS ANALYSIS

Fig. 5 shows path loss responses with distance for numerous mmWave and THz frequencies. It can be found that increasing either carrier frequency or distance causes increasing path loss. An interesting observation in mmWave and THz frequencies is that, in the low-frequency range of mmWave and THz, the rate of increase in path loss with distance is higher than that in the high-frequency range. For example, when moving from 28 GHz to 142 GHz, the rate of increase in path loss is higher than the increase in path loss rate when moving from 142 GHz to 250 GHz (Fig. 5). Given that path loss and capacity are directly related to each other, this can also be reflected in Fig. 6 where it can be found that the rate of decrease in average capacity per SCUE from 28 GHz to 142 GHz is higher than that when moving from 142 GHz to 250 GHz. This can be clarified by the fact that high-frequency signals usually undergo a less multipath fading effect resulting in fewer NLOS components or slight variations in channel characteristics.

Due to this high path loss rate in the low-frequency range (e.g., below 100 GHz), an increase in bandwidth in this range contributes more towards improving the system capacity

TABLE 3. Default simulation parameters and assumptions.

Parameters and Assumptions			Value
E-UTRA simulation case[1]			3GPP case 3
Cellular layout[2], Inter-site distance (ISD)[1,2], transmit direction			Hexagonal grid, dense urban, 3 sectors per macrocell, 1732 m, and downlink
Carrier frequency[2,3]			2 GHz NLOS for the macrocell and picocells, 28 GHz, 142 GHz, 250 GHz, and 300 GHz LOS for small cells
System bandwidth			10 MHz for each spectrum band
Number of apartments, SCBS distribution, and percentage of SCBSs per 3D cluster			98 per floor, dynamic, and 20%
Number of cells			1 macrocell, 2 picocells, 54 small cells per building (3-story building with 18 apartments per floor)
Total base station transmit power (dBm)			46 for macrocell[1], 37 for picocells[1], 5 for small cells[4] (operating at 28 GHz, 142 GHz, 250 GHz, and 300 GHz)
Co-channel small-scale fading model[1,6]			Frequency selective Rayleigh for 2 GHz, no small-scale fading for 28 GHz, 142 GHz, 250 GHz, and 300 GHz
External wall penetration loss[1] (L_{ow})			20 dB for 2 GHz
Path loss	Macrocell base station and a UE[1]	Outdoor macrocell UE	PL(dB) = 15.3 + 37.6log$_{10}R$, R is in m
		Indoor macrocell UE	PL(dB) = 15.3 + 37.6log$_{10}R$ + L_{ow}, R is in m
	Picocell base station and a UE[1]		PL(dB) = 140.7+36.7log$_{10}R$, R is in km
	SCBS and a UE[7,8]		$PL^{\mathrm{CI}} = \mathrm{FSPL}(f_C, 1\,\mathrm{m}) + 10n\log_{10}\left(\frac{d_{3\mathrm{D}}}{1\,\mathrm{m}}\right) + X_\sigma$ and $\mathrm{FSPL}(f_c, 1\mathrm{m}) = 32.4 + 20\log_{10}\left(\frac{f_c}{1\mathrm{GHz}}\right)$, where $d_{3\mathrm{D}}$ is the 3D separation distance between transmit and receive antennas in m, f_C is the carrier frequency in GHz, $\mathrm{FSPL}(f_c, 1\mathrm{m})$ is the free space path loss at f_C, n is the path loss exponent, and X_σ is the shadow fading in dB
Lognormal shadowing standard deviation (dB)			8 for macrocell base station[2], 10 for Picocell base station[1], (3.38 for 28 GHz, 2.89 for 142 GHz, 3.06 for 250 GHz, and 4.05 for 300 GHz) for SCBS[5,9]
Path loss exponent (n) for SCBSs[5,9]			1.90 for 28 GHz, 2.05 for 142 GHz, 2.27 for 250 GHz, and 2.32 for 300 GHz
Antenna configuration			Single-input single-output for all base stations and UEs
Antenna pattern (horizontal)			Directional (120^0) for macrocell base station[1], omnidirectional for Picocell base station[1] and SCBS[1] (for 2 GHz), and directional for SCBS[9] (for 28 GHz, 142 GHz, 250 GHz, and 300 GHz)
Base station antenna gain			14 for macrocell base station (dBi)[2], 5 for picocell base station (dBi)[1], and 23 for SCBS for 28 GHz, 142 GHz, 250 GHz, and 300 GHz (dBm)[4]
UE antenna gain[2,3,6,4]			0 dBi (for 2 GHz), 23 dBm (for 28 GHz, 142 GHz, 250 GHz, and 300 GHz)
UE noise figure[2,6,4] and UE speed[1]			9 dB (2 GHz) and 15 dB (for 28 GHz, 142 GHz, 250 GHz, and 300 GHz), 3 km/hr
Receiver thermal noise[4]			-69.2 dBm (for 28 GHz, 142 GHz, 250 GHz, and 300 GHz)
Total number of macrocell UEs			30
Picocell coverage and macrocell UEs offloaded to all picocells[1], indoor macrocell UEs[1]			40 m (radius), 2/15, 35%
3D multistory building and SCBS models: number of buildings, number of floors per building, number of apartments per floor, maximum number of SCBSs per apartment, percentage of apartments with SCBSs installed per 3D cluster of SCBSs, number of SCBSs per building, area of an apartment			L, 3, 98, 1, 0.2, 54, 10×10 m^2
Scheduler and traffic model[2]			PF and full buffer
Type of SCBSs			CSG femtocell base stations
TTI[1] and scheduler time constant (t_c)			1 ms and 100 ms
Total simulation run time			8 ms

taken [1]from [75], [2]from [76], [3]from [77], [4]from [78], from [5][79], from [6][80], from [7][45], from [8][46], from [9][52].

than when increasing bandwidth by the same amount in the high-frequency range (e.g., above 100 GHz). However, since more serviceable spectrum is usually available in the high-frequency range, enormous system capacity can be achieved in frequencies above 150 GHz.

C. SPECTRUM REUSE IN SMALL CELLS

1) SCENARIO 1

We consider a three-story building where each floor consists of 98 apartments. Recall that a maximum of one SCBS can be installed per apartment. Now, consider simulation scenario 1 where we assume an intra-floor interference threshold $\alpha_{\mathrm{tra}}^{\mathrm{opt}} = 0.3$. Now considering the lowest frequency of all mmWave and THz, i.e., 28 GHz, using Fig. 4, $\alpha_{\mathrm{tra}}^{\mathrm{opt}} = 0.3$ corresponds to a minimum distance of $d_{\mathrm{tra}}{*} = 28.15\ m$ required at the intra-floor level from the serving SCUE. This allows reusing the same spectrum in SCBSs, which are at least 3-tier (i.e., 3×10 m $= 30$ m) apart from the serving SCUE. It corresponds to a 2D cluster of 49 apartments at the intra-floor level that forms the RoE. However, for the inter-floor level, due to the high floor penetration loss at mmWave and THz frequencies, the same frequency can be reused in small cells on each floor such that a 3D cluster consists of $(49\times1) = 49$ apartments.

We consider CSG type of femtocell base stations for SCBSs, which are installed by end users. But in practice, probably, a great percentage of the total number of apartments may not have SCBSs installed. Unless it is installed by the MNO, it could be a rare situation that each apartment must be equipped with an SCBS. Considering this discussion, we assume that 20 percent of all the apartments per 3D cluster are installed with SCBSs. Based on estimating the minimum distance as aforementioned at the intra-floor level, there are 49 apartments per 2D cluster. So, the number of

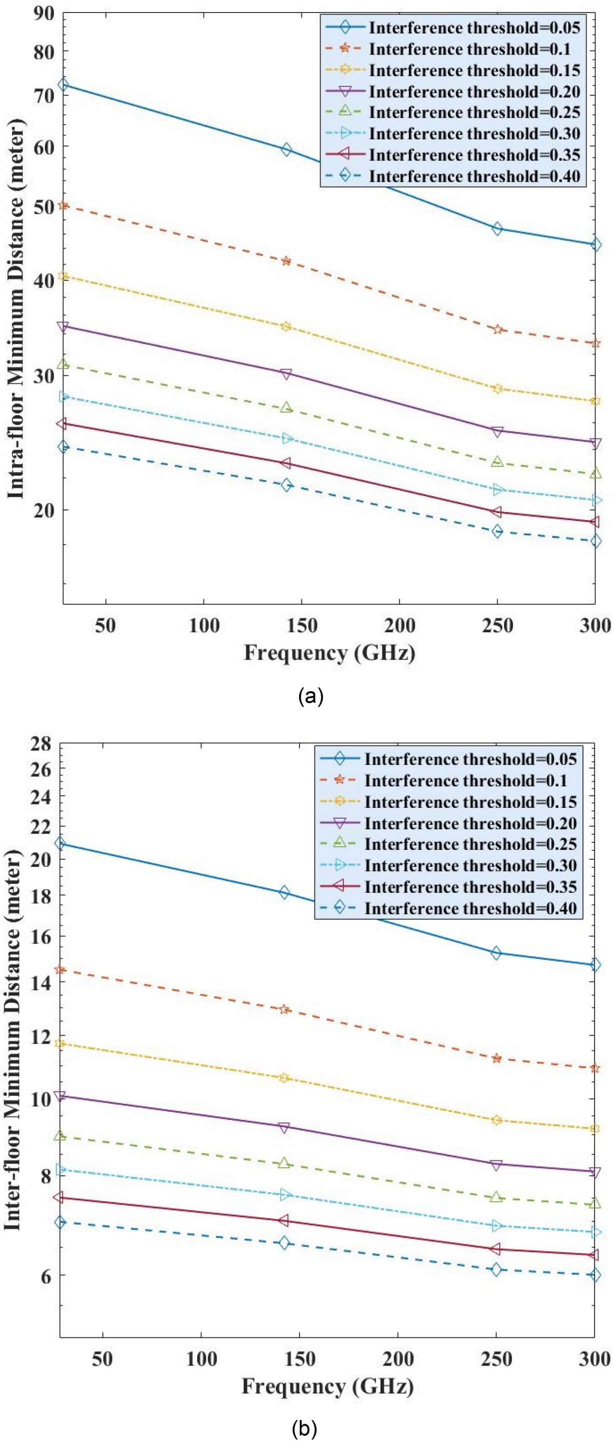

FIGURE 4. Minimum distance between co-channel small cells without incorporating internal wall or partition loss and floor penetration loss with a change in the interference threshold for frequencies ranging from 28 GHz to 300 GHz. (a) Intra-floor minimum distance and (b) Inter-floor minimum distance.

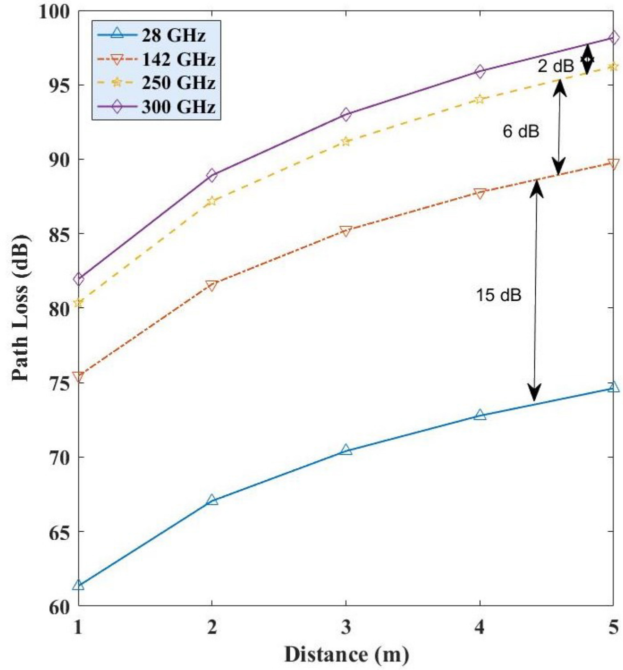

FIGURE 5. Pathloss versus distance at mmWave and THz frequencies.

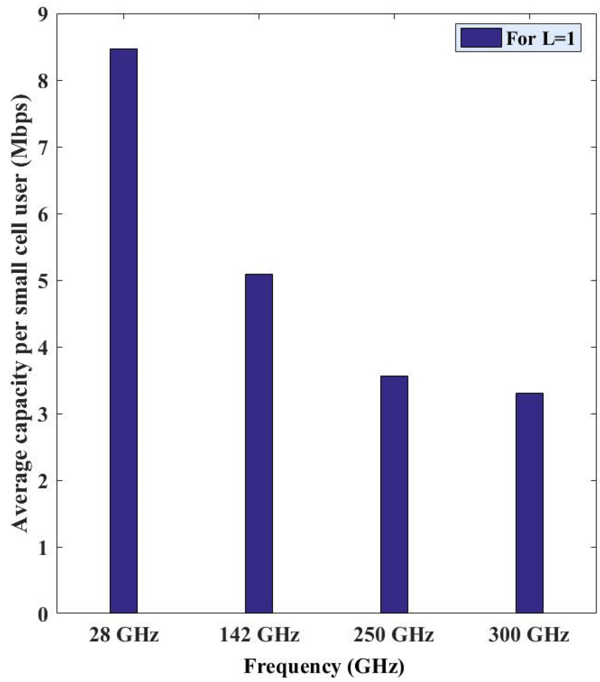

FIGURE 6. Average capacity per SCUE at mmWave and THz frequencies.

SCBSs per 2D cluster at the intra-floor level is $0.2 \times 49 \approx 9$. Since there are 98 apartments per floor and three floors per building, the number of 2D clusters per floor is $(98/49) = 2$ and hence, per three-story building is $(2 \times 3) = 6$. Since spectrum resources can be reused in SCBSs on each floor of the building, the number of SCBSs per 3D cluster is $(9 \times 1) = 9$ and per three-story building is $(6 \times 9) = 54$.

Recall that there are two 2D clusters of apartments per floor each consisting of 9 small cells resulting in a total of 54 small cells per building. Assume case 1 such that no macrocell spectrum is considered to be reused in small cells. 2 GHz microwave spectrum is used to schedule traffic

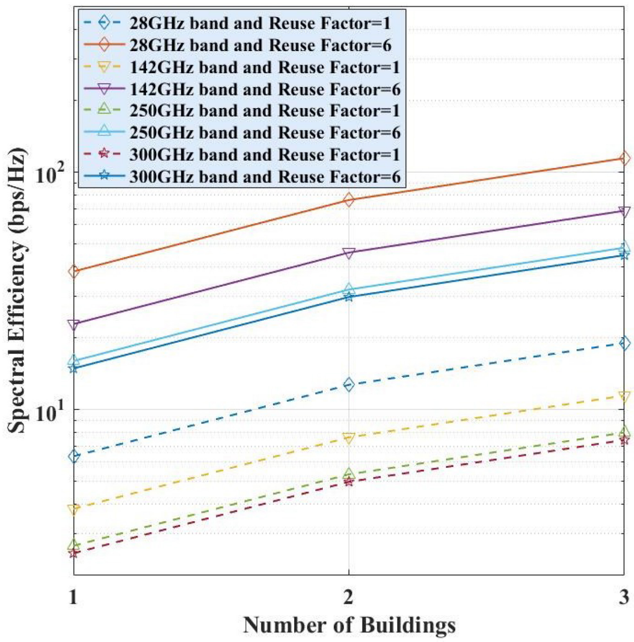

FIGURE 7. SE performance versus spectrum reuse factor when considering small cells only under scenario 1.

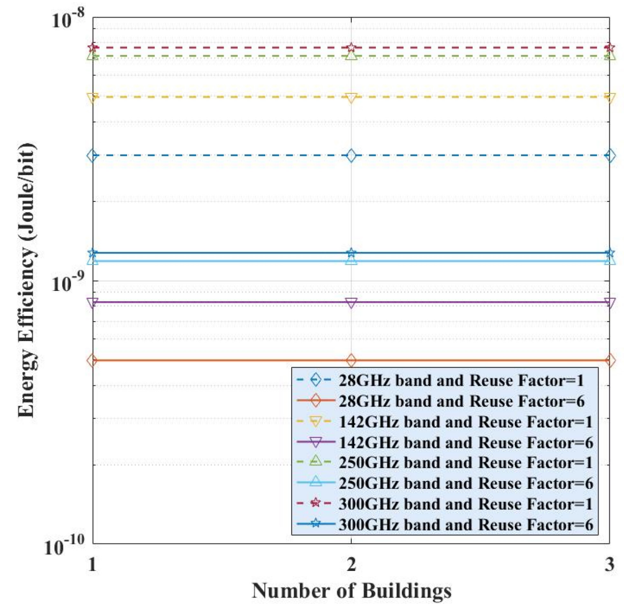

FIGURE 8. EE performance versus spectrum reuse factor when considering small cells only under scenario 1.

of macrocells and picocells, whereas mmWave and THz spectrum is used to schedule traffic of small cells per 3D cluster within each building. Now under scenario 1, we evaluate the spectrum resource reuse depending on whether or not the same spectrum resources are reused in small cells. Because both SE and EE relate directly to the capacity, SE and EE show a similar response to Fig. 6. More specifically, irrespective of the reuse of resources, the rate of increase in the system level SE and EE is low in the high-frequency range, whereas, the rate of increase in SE and EE is high in the low-frequency range (Figs. 7-10) of mmWave and THz frequency bands.

It is to be noted that with reusing spectrum resources in small cells, the overall (when considering all types of cells, including the macrocell, picocells, and small cells) responses of SE and EE (Figs. 9-10) are degraded in comparison with when considering the SE and EE performance metrics of only small cells (Figs. 7-8). This can be clarified by the fact that because of the poor channel conditions at the 2 GHz microwave frequency, the average SE (bps per Hz) achieved by both the macrocell and picocells is much lower than that obtained by in-building small cells alone for the same spectrum bandwidth. Likewise, because both macrocells and picocells usually operate at a higher transmission power than small cells do, the average EE when considering only small cells outperforms the overall system level EE obtained when considering the macrocell and picocells in addition to small cells. Besides, SE and EE increase with an increase in the spectrum reuse factor for small cells (Figs. 7-10). Hence, as we increase the spectrum reuse factor, both SE and EE improve accordingly, leading to a condition that any required SE and EE performances can be obtained.

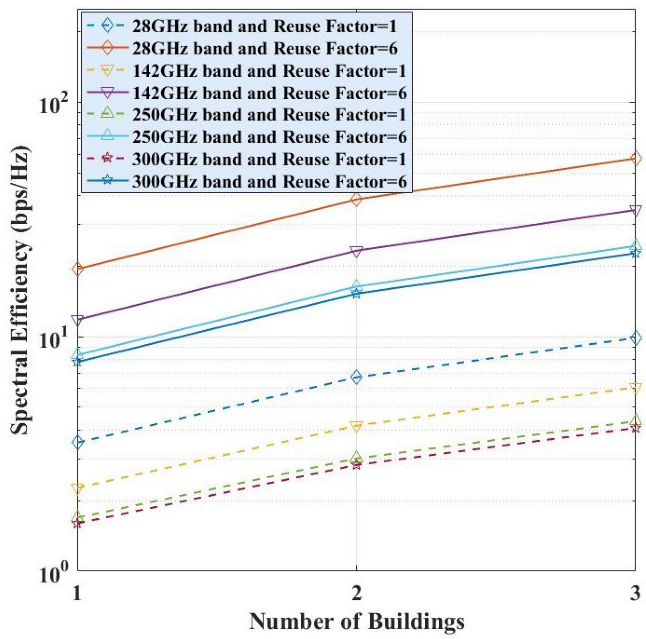

FIGURE 9. SE performance versus spectrum reuse factor when considering the macrocell, picocells, and small cells under scenario 1.

2) SCENARIO 2

The performance of scenario 2 with respect to scenario 1 as well as spectrum reuse factor = 1 is shown below (Figs. 11-13) for $\alpha_{\text{tra}}^{\text{opt}} = 0.35$. The corresponding minimum distance requirement at the intra-floor level to enforce $\alpha_{\text{tra}}^{\text{opt}} = 0.35$is given by 25.95 m for 28 GHz, 23.00 m for 142 GHz, 19.84 m for 250 GHz, and 19.26 m for 300 GHz. These minimum distances correspond to a RoE at the

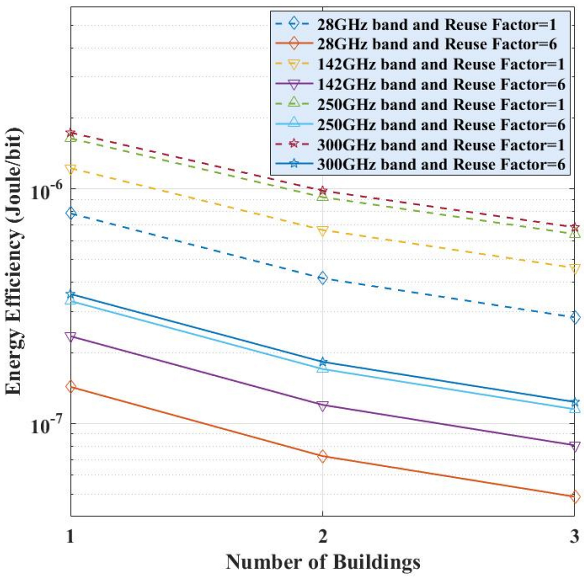

FIGURE 10. EE performance versus spectrum reuse factor when considering the macrocell, picocells, and small cells under scenario 1.

intra-floor level, and hence a 3D cluster, of 49, 49, 25, and 25 apartments, respectively, for 28 GHz, 142 GHz, 250 GHz, and 300 GHz bands. As mentioned before, the above calculations also imply that different frequency bands need different sizes of 3D clusters. In what follows, we carry out extensive simulation and show a relative comparison between scenario 2 with scenario 1, along with reuse factor = 1 as a default scenario.

3) COMPARATIVE ANALYSIS

As shown in Figs. 11-12, in scenario 1, SE and EE responses of all bands are improved by 6 times as compared to that in reuse factor = 1. When comparing responses of SE and EE of all bands in scenario 2, it can be found in Figs. 11(a)-11(b) that there is no further improvement in SE and EE over scenario 1 at 28 GHz and 142 GHz bands. This is because the spectrum of 28 GHz and 142 GHz bands cannot be reused more in scenario 2 than in scenario 1 due to satisfying the minimum distance requirement. In contrast, SE and EE performances of 250 GHz and 300 GHz bands are improved by 6 times in scenario 1 as compared to that in reuse factor = 1, which are improved further in scenario 2, particularly, by 11.76 times as compared to their performances in reuse factor = 1. This is because of reusing the spectrum of 250 GHz and 300 GHz bands in scenario 2 by about ((11.76-6)/6) 96% more than that in scenario 1. Hence, unlike 28 GHz and 142 GHz bands, 250 GHz and 300 GHz bands provide better SE and EE performances in scenario 2 than their performances in scenario 1 as shown in Figs. 11(a)-11(b) for a single building of SCBSs and in Figs. 12(a)-12(b) for multiple buildings of SCBSs. These observations imply that to achieve the best out of spectrum reuse to in-building small cells, choosing RoE should be frequency band specific, instead of considering the same RoE (corresponding to the lowest frequency bands of all) for all frequency bands in multi-band-enabled in-building SCBSs.

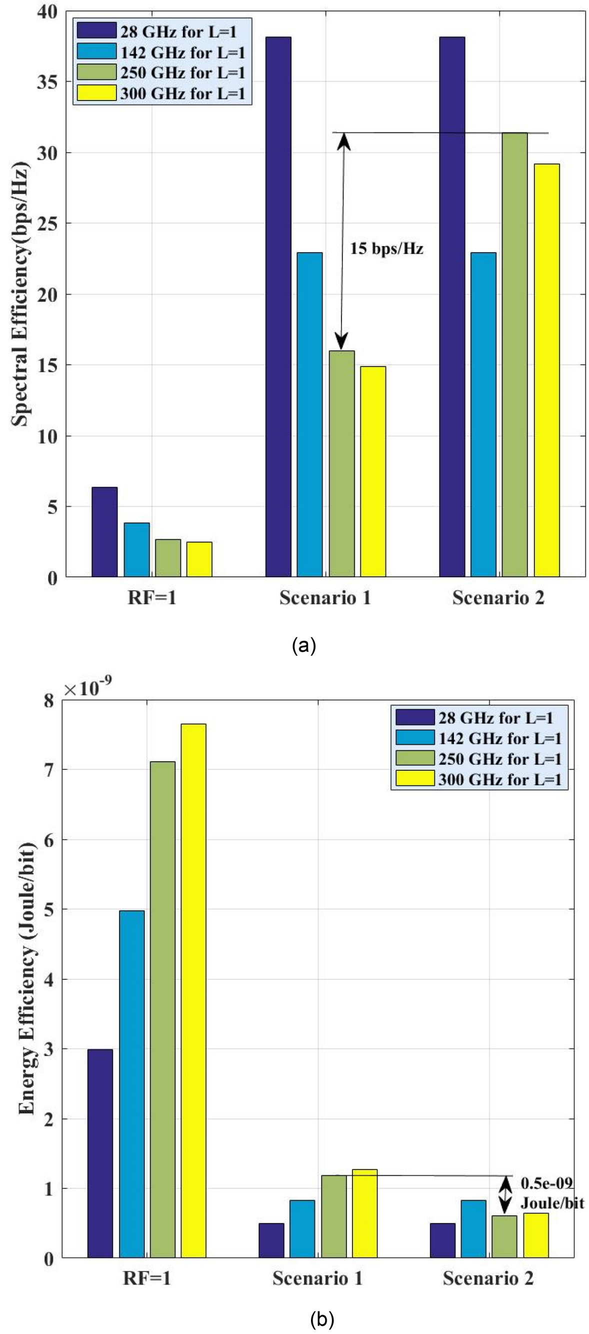

FIGURE 11. (a) SE and (b) EE performances of numerous mmWave and THz bands under different scenarios for $L = 1$, where RF represents the reuse factor.

Further, from Figs. 11 and 12, it can be found that SE and EE at 28 GHz are much higher than that at 142 GHz, 250 GHz, and 300 GHz. This indicates that to achieve the same 28 GHz SE and EE performances, more spectrum bandwidth than that required by the 28 GHz band is needed by these high-frequency bands, including 142 GHz, 250 GHz, and 300 GHz. Because high-frequency bands can be reused more to in-building SCBSs, and there is a huge amount of unused bandwidth available in the high-frequency

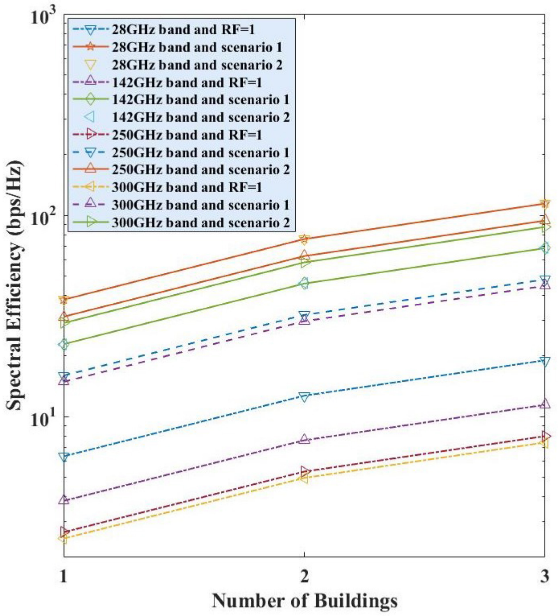

(a)

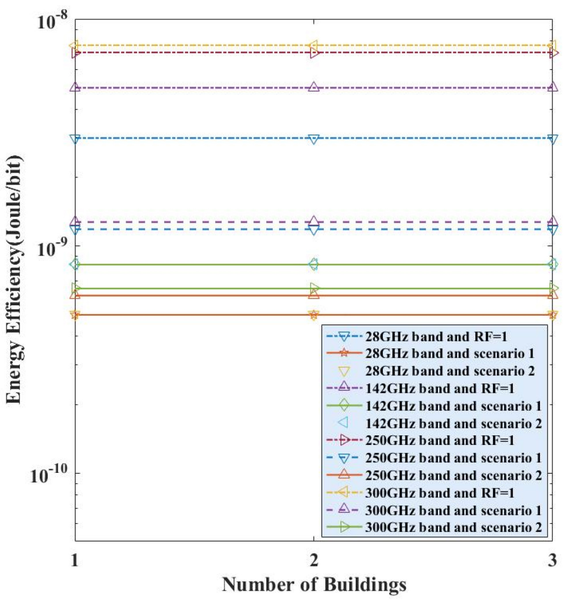

(b)

FIGURE 12. (a) SE and (b) EE performances of numerous mmWave and THz bands under different scenarios for L>1.

THz bands, SE and EE performances at these high-frequency THz bands (i.e., 142 GHz, 250 GHz, and 300 GHz) can be enhanced.

Furthermore, when considering the total contribution from all spectrum bands of 28 GHz, 142 GHz, 250 GHz, and 300 GHz of any SCBS, the SE is improved by about 8 times in scenario 2 as compared to that in the scenario of reuse factor = 1 per building of SCBSs (Fig. 13(a)). This implies an improvement in SE in scenario 2 over that in scenario 1 by ((8-6)/6 = 33.33%). Likewise, EE performance in scenario 2 is improved by 87.5% as compared to that for reuse factor = 1, which is also an improvement of 4.5% over

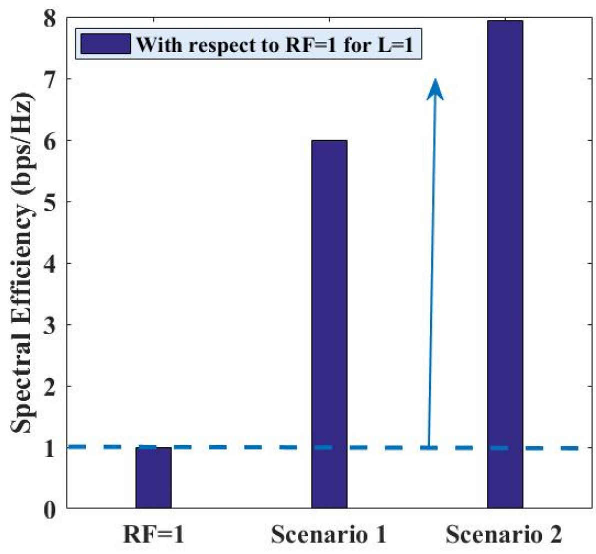

(a)

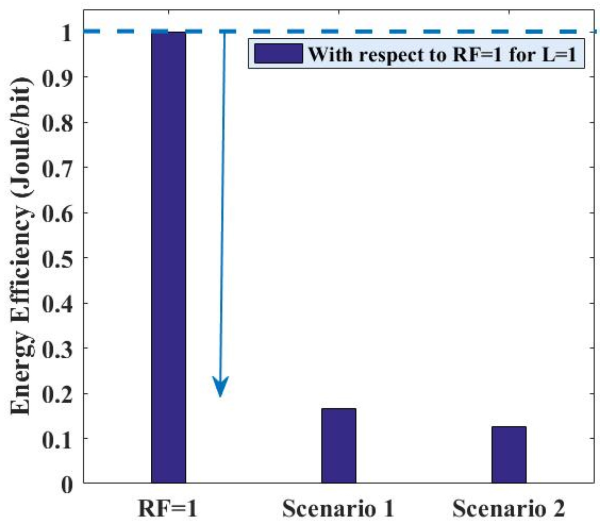

(b)

FIGURE 13. (a) Aggregate SE and (b)aggregate EE performances of all mmWave and THz bands under different scenarios for $L = 1$.

that in scenario 1 (Figure 13(b)). This result also suggests considering each frequency band separately when defining a 3D cluster of multi-band-enabled SCBSs.

In summary, spectrum resource reuse plays a significant role when it is a matter of improving SE and EE responses of in-building small cells. Moreover, if SCBSs are enabled with multiple frequency bands, low-frequency bands usually provide high SE and EE performances. In addition, the RoE should be defined per frequency band to get the best SE and EE responses of small cells in a building at the cost of an additional complexity level.

4) PERFORMANCE COMPARISON

It is expected that the 6G mobile will serve 10 times the average SE [84] (i.e., 270-370 bps/Hz), as well as

10 times the average EE [85] (i.e., 0.3×10^{-6} Joules/bit), of the 5G mobile systems [86], [87]. Usually, frequency spectrum, including mmWave and THz, can be reused in small cells within a building (termed vertical intra-building spectrum reuse) and small cells in adjacent buildings (termed horizontal inter-building spectrum reuse). Hence, the spectrum reuse factor can be varied by changing the number of times the mmWave and THz spectrum can be reused per building and the number of buildings L over the macrocell coverage. Fig. 14 shows SE and EE performances of the proposed generic model with the variation of the reuse factor per building and the number of buildings under scenarios 1 and 2. As it can be found that, with reuse factor = 12 per building, the minimum and maximum SE requirements for the 6G mobile mentioned above can be satisfied under scenario 2 for $L = 5$ to 7 and scenario 2 for $L = 6$ to 9. Hence, the 6G SE requirement can be satisfied by choosing appropriate values of L and spectrum reuse factor per building. Note that with the default scenario of a reuse factor of 1 per building, the number of buildings required to satisfy the SE requirement of 6G is very large, and it is not unusual that satisfying the SE requirement of 6G may not be possible in some cases. However, from Fig. 14(b), the EE requirement of 6G mobile, 0.3×10^{-6} Joules/bit, can be easily satisfied under all scenarios including the default one.

VII. CONCLUSION

This paper has presented a generic model to reuse a wide range of spectrum in the mmWave and THz frequencies in in-building small cells. For mmWave and THz frequency bands, we have considered 28 GHz, 142 GHz, 250 GHz, and 300 GHz bands, and each small cell has been considered enabling with these multiple bands. We have considered both static (i.e., a small cell per apartment) and random (i.e., an apartment may not have a small cell) distributions of small cells within each 3D cluster. Moreover, two scenarios where in scenario 1, the same size of the 3D cluster for all frequency bands, and in scenario 2, different sizes of the 3D cluster each corresponding to a different frequency band, have been considered.

It has been found that the minimum distance requirement between co-channel small cells decreases with an increase in the interference threshold at the SCUE, which in turn increases the spectrum reuse factor. The reduction rate in average capacity per SCUE from 28 GHz to 142 GHz has been found higher than that when moving from 142 GHz to 250 GHz since high-frequency signals usually undergo less multipath fading effect. Further, SE and EE have been found to increase with an increase in the spectrum reuse factor.

When each small cell has operated at all four frequency bands, the overall SE has been improved by about 8 times in scenario 2 for reuse factor = 1 as compared to an improvement of 6 times in scenario 1, indicating an improvement in SE in scenario 2 over what in scenario 1 by 33.33%. Likewise, EE in scenario 2 has been improved by 4.5% over what in scenario 1. These results suggest considering each frequency band separately when defining a 3D cluster of multi-band-enabled SCBSs, i.e., considering scenario 2 over scenario 1. Finally, it has been shown that the proposed generic reuse model can achieve the prospective SE and EE requirements for 6G mobile systems by choosing appropriate values of the number of times the mmWave and THz spectrum is reused to small cells per multi-floor building and the number of buildings over the macrocell coverage under both scenario 1 and scenario 2.

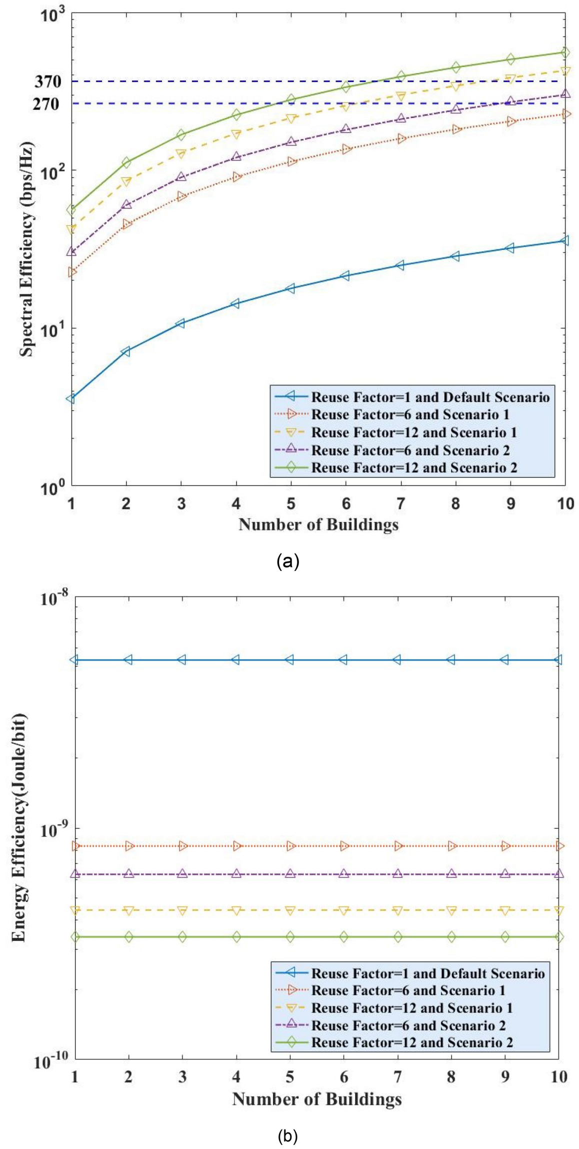

FIGURE 14. (a) SE and (b) EE with the variation of the number of buildings and reuse factor per building under scenarios 1 and 2.

REFERENCES

[1] P. F. Acts, *World Radiocommunication Conference (WRC-15)*, ITU, Geneva, Switzerland, 2015.
[2] *Provisional Final Acts*, ITU, Geneva, Switzerland, 2019
[3] F. Boccardi, R. W. Heath, A. Lozano, T. L. Marzetta, and P. Popovski, "Five disruptive technology directions for 5G," *IEEE Commun. Mag.*, vol. 52, no. 2, pp. 74–80, Feb. 2014.

[4] S. Tripathi, N. V. Sabu, A. K. Gupta, and H. S. Dhillon, "Millimeter-wave and terahertz spectrum for 6G wireless," in *6G Mobile Wireless Networks. Computer Communications and Networks*. Cham, Switzerland: Springer, 2021. [Online]. Available: https://doi.org/10.1007/978-3-030-72777-2_6

[5] J. G. Andrews, S. Buzzi, W. Choi, S. V. Hanly, A. Lozano, and A. C. K. Soong, "What will 5G be?" *IEEE J. Sel. Areas Commun.*, vol. 32, no. 6, pp. 1065–1082, Jun. 2014.

[6] J. G. Andrews, T. Bai, M. N. Kulkarni, A. Alkhateeb, A. K. Gupta, and R. W. Heath, "Modeling and analyzing millimeter wave cellular systems," *IEEE Trans. Commun.*, vol. 65, no. 1, pp. 403–430, Jan. 2017.

[7] I. A. Hemadeh, K. Satyanarayana, M. El-Hajjar, and L. Hanzo, "Millimeter-wave communications: Physical channel models, design considerations, antenna constructions, and link-budget," *IEEE Commun. Surveys Tuts.*, vol. 20, no. 2, pp. 870–913, 2nd Quart., 2018.

[8] S. Rangan, T. S. Rappaport, and E. Erkip, "Millimeter-wave cellular wireless networks: Potentials and challenges," *Proc. IEEE*, vol. 102, no. 3, pp. 366–385, Mar. 2014.

[9] F. Khan, Z. Pi, and S. Rajagopal, "Millimeter-wave mobile broadband with large scale spatial processing for 5G mobile communication," in *Proc. IEEE 50th Annu. Allerton Conf. Commun. Control Comput. (Allerton)*, 2012, pp. 1517–1523.

[10] R. Sun, P. B. Papazian, J. Senic, C. Gentile, and K. A. Remley, *Angle and Delay-Dispersion Characteristics in a Hallway and Lobby at 60 GHz*, NIST, Gaithersburg, MD, USA, 2018.

[11] R. Sun, C. A. Gentile, J. Senic, P. Vouras, P. B. Papazian, and N. T. Golmie, "Millimeter-wave radio channels vs. Synthetic beamwidth," *IEEE Commun. Mag.*, vol. 56, no. 12, pp. 53–59, Dec. 2018.

[12] Y. Niu, Y. Li, D. Jin, L. Su, and A. V. Vasilakos, "A survey of millimeter wave (mmWave) communications for 5G: Opportunities and challenges," *J. Wireless Netw.*, vol. 21, no. 8, pp. 2657–2676, 2015.

[13] I. F. Akyildiz, J. M. Jornet, and C. Han, "Terahertz band: Next Frontier for wireless communications," *J. Phys. Commun.*, vol. 12, pp. 16–32, Sep. 2014.

[14] R. Singh and D. Sicker, "Parameter modeling for small-scale mobility in indoor THz communication," in *Proc. GLOBECOM*, Waikoloa, HI, USA, 2019, pp. 1–6, doi: 10.1109/GLOBECOM38437.2019.9013838.

[15] C. Han et al., "Terahertz communications (TeraCom): Challenges and impact on 6G wireless systems," Dec. 2019, *arXiv:1912.06040*.

[16] W. Saad, M. Bennis, and M. Chen, "A vision of 6G wireless systems: Applications, trends, technologies, and open research problems," *IEEE Netw.*, vol. 34, no. 3, pp. 134–142, May/Jun. 2020.

[17] H. U. Tahseen, L. Mescia, and L. Catarinucci, "A survey of five generations of MIMO multiband base station antennas," *Radio Sci.*, vol. 58, no. 7, 2023, Art. no. e2023RS007725.

[18] S. I. Siddiqui, S. Bashir, A. Khan, S. Ghafoor, and I. Aziz, "A dual-band high-gain beam steering antenna array for 5G sub-6 GHzbase station," *Sci. Rep.*, vol. 14, Jan. 2024, Art. no. 26517.

[19] Y. Zhao et al., "A compact dual-broadband multiple-input multiple-output (MIMO) indoor base station antenna for 2G/3G/LTE systems," *IEEE Access*, vol. 7, pp. 82238–82245, 2019.

[20] A. Alieldin et al., "A triple-band dual-polarized indoor base station antenna for 2G, 3G, 4G and sub-6 GHz5G applications," *IEEE Access*, vol. 6, pp. 49209–49216, 2018.

[21] A. A. Yussuf and S. Paker, "Dual-band ViVaLDI MIMO antennas designed for sub-6 GHz 5G wireless applications," in *Proc. Int. Conf. Broadband Commun. Next Gener. Netw. Multimedia Appl. (CoBCom)*, Graz, Austria, 2024, pp. 1–4.

[22] H.-T. Chou and Z.-D. Yan, "Antenna-in-package of lateral cross-dipole elements for end-fire dual-polarized radiation at dual millimeter-wave frequency bands for 5G FR2 user equipment applications," *IEEE Trans. Antennas Propag.*, early access, Nov. 14, 2024, doi: 10.1109/TAP.2024.3494048.

[23] C. R. Jetti et al., "Design of dual band mmWave multiple-input–multiple-output (MIMO) antenna for future wireless applications," in *Proc. IEEE Wireless Antenna Microw. Symp. (WAMS)*, Ahmedabad, India, 2023, pp. 1–4.

[24] R. K. Saha, "Spectrum sharing in satellite-mobile multisystem using 3-D in-building small cells for high spectral and energy efficiencies in 5G and beyond era," *IEEE Access*, vol. 7, pp. 43846–43868, 2019.

[25] R. K. Saha, "An overview and mechanism for the coexistence of 5G NR-U (new radio unlicensed) in the millimeter-wave spectrum for indoor small cells," *Wireless Commun. Mobile. Comput.*, vol. 2021, no. 1, Sep. 2021, Art. no. 8661797.

[26] M. Hajir and F. Gagnon, "Spatial reuse model for mmWave frequencies in ultra dense small-cells networks," in *Proc. IEEE 28th Annu. Int. Symp. Pers. Indoor Mobile Radio Commun. (PIMRC)*, Montreal, QC, Canada, 2017, pp. 1–7, doi: 10.1109/PIMRC.2017.8292166.

[27] X. Zhou, S. Feng, Y. Ding, Y. Liu, Y. Wang, and Y. Zhang, "Game-theoretical frequency reuse method for complex cognitive femto-cell network," in *Proc. 8th Int. Conf. Commun. Netw. China (CHINACOM)*, 2013, pp. 318–322, doi: 10.1109/ChinaCom.2013.6694613.

[28] J. Feng and M. Tao, "Hypergraph-based frequency reuse in dense femtocell networks," in *Proc. IEEE/CIC Int. Conf. Commun. China (ICCC)*, Xi'an, China, 2013, pp. 537–542, doi: 10.1109/ICCChina.2013.6671173.

[29] J. Liu, J. Y. Wu, J. Chen, P. Wang, and J. Zhang, "Radio resource allocation in buildings with dense femtocell deployment," in *Proc. 21st Int. Conf. Comput. Commun. Netw. (ICCCN)*, Munich, Germany, Jul./Aug. 2012, pp. 1–5.

[30] X. Wang, W. Zheng, Z. Lu, X. Wen, and W. Li, "Dense femtocell networks power self-optimization: An exact potential game approach," *Int. J. Commun. Syst.*, vol. 29, no. 1, pp. 16–32, 2016.

[31] C. Jiming, W. Peng, and Z. Jie, "Adaptive soft frequency reuse scheme for in-building dense femtocell networks," *China Commun.*, vol. 10, no. 1, pp. 44–55, Jan. 2013, doi: 10.1109/CC.2013.6457529.

[32] Z. Liu, T. B. Sorensen, and P. E. Mogensen, "Site-specific study of in-building wireless solutions with Poisson traffic," in *Proc. IEEE Veh. Technol. Conf. (VTC Fall)*, San Francisco, CA, USA, 2011, pp. 1–5, doi: 10.1109/VETECF.2011.6093062.

[33] C. Bouras, G. Diles, V. Kokkinos, and A. Papazois, "Transmission optimizing on dense femtocell deployments in 5G," *Int. J. Commun. Syst.*, vol. 29, no. 16, pp. 2388–2402, 2016.

[34] S. J. Kao and H. L. Wang, "Dynamic orthogonal frequency division multiple access resource management for downlink interference avoidance in two-tier networks," *Int. J. Commun. Syst.*, vol. 28, no. 2, pp. 81–295, 2015.

[35] R. Langar, S. Secci, R. Boutaba, and G. Pujolle, "An operations research game approach for resource and power allocation in cooperative femtocell networks," *IEEE Trans. Mobile Comput.*, vol. 14, no. 4, pp. 675–687, Apr. 2015.

[36] N. Saquib, E. Hossain, and D. Kim, "Fractional frequency reuse for interference management in LTE-advanced HetNets," *IEEE Wireless Commun.*, vol. 20, no. 2, pp. 113–122, Apr. 2013.

[37] X. Wang, Q. Han, X. Guan, and K. Ma, "Price-based interference management in dense femtocell systems," *Int. J. Commun. Syst.*, vol. 28, no. 1, pp. 19–37, 2015.

[38] S. E. Nai and T. Q. S. Quek, "Coexistence in two-tier femtocell networks: Cognition and optimization," in *Proc. Int. Conf. Comput. Netw. Commun. (ICNC)*, Maui, HI, USA, 2012, pp. 655–659, doi: 10.1109/ICCNC.2012.6167504.

[39] I. Hwang, B. Song, and S. S. Soliman, "A holistic view on hyper-dense heterogeneous and small cell networks," *IEEE Commun. Mag.*, vol. 51, no. 6, pp. 20–27, Jun. 2013.

[40] S.-R. Cho and W. Choi, "Energy-efficient repulsive cell planning for heterogeneous cellular networks," *IEEE J. Sel. Areas Commun.*, vol. 31, no. 5, pp. 870–882, Sep. 2014.

[41] S.-R. Cho and W. Choi, "Coverage and load balancing in heterogeneous cellular networks with minimum cell separation," *IEEE Trans. Mobile Comput.*, vol. 13, no. 9, pp. 1955–1966, Sep. 2014.

[42] R. K. Saha and C. Aswakul, "A tractable analytical model for interference characterization and minimum distance enforcement to reuse resources in three-dimensional in-building dense small cell networks." *Int. J. Commun. Syst.*, vol. 30, no. 11, 2017, Art. no. e3240. [Online]. Available: https://doi.org/10.1002/dac.3240

[43] R. K. Saha, "Modeling interference to reuse millimeter-wave spectrum to in-building small cells toward 6G," in *Proc. IEEE 92nd Veh. Technol. Conf. (VTC-Fall)*, Victoria, BC, Canada, 2020, pp. 1–7, doi: 10.1109/VTC2020-Fall49728.2020.9348747.

[44] R. K. Saha, "Spectrum reuse in the terahertz band for in-building small cell networks," in *Proc. 20th Int. Conf. Netw. (ICN)*, 2021, pp. 30–35.

[45] S. Ju et al., "Millimeter wave and sub-terahertz spatial statistical channel model for an indoor office building," *IEEE J. Sel. Areas Commun.*, vol. 39, no. 6, pp. 1561–1575, Jun. 2021.

[46] *Study on Channel Model for Frequencies From 0.5 to 100 GHz*, 3GPP Standard 38.901, Dec. 2019.

[47] *Simulation Assumptions and Parameters for FDD HeNB RF Requirements*, 3GPP, Sophia Antipolis, France, May 2009.

[48] *Simulation Assumptions and Parameters for FDD HeNB RF Requirements*, 3GPP, Sophia Antipolis, France, Mar. 2009.

[49] R. K. Saha, S. Nanba, and K. Nishimura, "A technique for cloud based clustering and spatial resource reuse and scheduling of 3-D in-building small cells using CoMP for high capacity CRAN," *IEEE Access*, vol. 6, pp. 71602–71621, 2018.

[50] D. Chen, T. Jiang, and Z. Zhang, "Frequency partitioning methods to mitigate cross-tier interference in two-tier femtocell networks," *IEEE Trans. Veh. Technol.*, vol. 64, no. 5, pp. 1793–1805, May 2015.

[51] A. Tukmanov, Z. Ding, S. Boussakta, and A. Jamalipour, "On the impact of network geometric models on multicell cooperative communication systems," *IEEE Wireless Commun.*, vol. 20, no. 1, pp. 75–81, Feb. 2013.

[52] Y. Xing, T. S. Rappaport, and A. Ghosh, "Millimeter wave and sub-THz indoor radio propagation channel measurements, models, and comparisons in an office environment," *IEEE Commun. Lett.*, vol. 25, no. 10, pp. 3151–3155, Oct. 2021, doi: 10.1109/LCOMM.2021.3088264.

[53] Y. Xing and T. S. Rappaport, "Spectrum coexistence between systems in space and on the ground at frequencies above 100 GHz(Invited)," *IEEE Commun. Lett.*, vol. 23, no. 1, p. 342, Dec. 2022.

[54] T. S. Rappaport et al., "Wireless communications and applications above 100 GHz: Opportunities and challenges for 6G and beyond," *IEEE Access*, vol. 7, pp. 78729–78757, 2019. doi: 10.1109/ACCESS.2019.2921522.

[55] S. Sun et al., "Investigation of prediction accuracy, sensitivity, and parameter stability of large-scale propagation path loss models for 5G wireless communications," *IEEE Trans. Veh. Technol.*, vol. 65, no. 5, pp. 2843–2860, May 2016.

[56] T. S. Rappaport, *wireless Communications: Principles and Practice*, 2nd ed. Upper Saddle River, NJ, USA: Prentice-Hall, 2002.

[57] T. S. Rappaport, G. R. MacCartney, M. K. Samimi, and S. Sun, "Wideband millimeter-wave propagation measurements and channel models for future wireless communication system design," *IEEE Trans. Commun.*, vol. 63, no. 9, pp. 3029–3056, Sep. 2015.

[58] S. Sun, T. A. Thomas, T. S. Rappaport, H. Nguyen, I. Z. Kovács, and I. Rodriguez, "Path loss, shadow fading, and line-of-sight probability models for 5G urban macro-cellular scenarios," in *Proc. IEEE Globecom Workshops (GC Wkshps)*, Dec. 2015, pp. 1–7.

[59] T. S. Rappaport et al., *Millimeter Wave Wireless Communications*. London, U.K.: Pearson, 2015.

[60] G. R. MacCartney, T. S. Rappaport, S. Sun, and S. Deng, "Indoor office wideband millimeter-wave propagation measurements and channel models at 28 and 73 GHzfor ultra-dense 5G wireless networks," *IEEE Access*, vol. 3, pp. 2388–2424, 2015.

[61] M. K. Samimi, T. S. Rappaport, and G. R. MacCartney, "Probabilistic omnidirectional path loss models for millimeter-wave outdoor communications," *IEEE Wireless Commun. Lett.*, vol. 4, no. 4, pp. 357–360, Aug. 2015.

[62] Z. Kaleem, B. Hui, and K. H. Chang, "QoS priority-based dynamic frequency band allocation algorithm for load balancing and interference avoidance in 3GPP LTE HetNet," *EURASIP J. Wireless Commun. Netw.*, vol. 185, pp. 1–18, Nov. 2014.

[63] B. Kim, S. Malik, S. Moon, C. You, H. Liu, J.-H. Kim, and I. Hwang, "Performance analysis of coordinated multipoint with scheduling and precoding schemes in the LTE-A system," *Wireless Pers. Commun.*, vol. 77, pp. 2615–2630, Feb. 2014.

[64] W. Kim, Z. Kaleem, and K. H. Chang, "Power headroom report-based uplink power control in 3GPP LTE-A HetNet," *EURASIP J. Wireless Commun. Netw.*, vol. 233, pp. 1–13., Oct. 2015.

[65] R. K. Saha and P. Saengudomlert, "Novel resource scheduling for spectral efficiency in LTE-advanced systems with macrocells and femtocells," in *Proc. 8th Int. Conf. Elect. Eng. Electron. Comput. Telecommun. Inf. Technol. (ECTI-CON)*, May 2011, pp. 340–343.

[66] T. K. Vu, S. Kwon, and S. Oh, "Cooperative interference mitigation algorithm in heterogeneous network," *IEICE Trans. Commun.*, vol. E98-B, no. 11, pp. 2238–2247, 2015.

[67] H. Hashemi, "The indoor radio propagation channel," *Proc. IEEE*, vol. 81, no. 7, pp. 943–968, Jun. 1993.

[68] C. Han et al., "Molecular absorption effect: A double-edged sword of terahertz communications," *IEEE Wireless Commun.*, vol. 30, no. 4, pp. 140–146, Aug. 2023.

[69] C. Han, A. O. Bicen, and I. F. Akyildiz, "Multi-wideband waveform design for distance-adaptive wireless communications in the terahertz band," *IEEE Trans. Signal Process.*, vol. 64, no. 4, pp. 910–922, Feb. 2016.

[70] Z. Hossain and J. M. Jornet, "Hierarchical bandwidth modulation for ultra-broadband terahertz communications," in *Proc. IEEE Int. Conf. Commun. (ICC)*, Shanghai, China, 2019, pp. 1–7.

[71] J. M. Jornet and I. F. Akyildiz, "Channel modeling and capacity analysis for electromagnetic wireless nanonetworks in the terahertz band," *IEEE Trans. Wireless Commun.*, vol. 10, no. 10, pp. 3211–3221, Oct. 2011.

[72] H. Zheng, J. Zhang, H. Hu, and J. Zhang, "The analysis of indoor wireless communications by a blockage model in ultra-dense networks," in *Proc. IEEE 88th Veh. Technol. Conf. (VTC-Fall)*, Chicago, IL, USA, 2018, pp. 1–6.

[73] S. Wu, C. Chakrabarti, and A. Alkhateeb, "Proactively predicting dynamic 6G link blockages using LiDAR and in-band signatures," *IEEE Open J. Commun. Soc.*, vol. 4, pp. 392–412, 2023.

[74] T. Bai, R. Vaze, and R. W. Heath, "Analysis of blockage effects on urban cellular networks," *IEEE Trans. Wireless Commun.*, vol. 13, no. 9, pp. 5070–5083, Sep. 2014.

[75] *Evolved Universal Terrestrial Radio Access (E-UTRA); Radio Frequency (RF) System Scenarios*, 3GPP Standard 36.942, Jul. 2007, Accessed: Feb. 15, 2020. [Online]. Available: https://portal.3gpp.org/desktopmodules/Specifications/Specification/Details.aspx?specificationId=2592

[76] 3GPP, *Simulation Assumptions and Parameters for FDD HeNB RF Requirements*, document TSG RAN WG4 (Radio) Meeting #51, R4-092042, 3GPP, Sophia Antipolis, France, May 2009. [Online]. Available: https://www.3gpp.org/ftp/tsg_ran/WG4_Radio/TSGR4_51/Documents/

[77] S. Geng, J. Kivinen, X. Zhao, and P. Vainikainen, "Millimeter-wave propagation channel characterization for short-range wireless communications," *IEEE Trans. Veh. Technol.*, vol. 58, no. 1, pp. 3–13, Jan. 2009.

[78] K. Rikkinen et al., "THz radio communication: Link budget analysis toward 6G," *IEEE Commun. Mag.*, vol. 58, no. 11, pp. 22–27, Nov. 2020, doi: 10.1109/MCOM.001.2000310.

[79] P. Tang et al., "Channel measurement and path loss modeling from 220 GHz to 330 GHz for 6G wireless communications," *China Commun.*, vol. 18, no. 5, pp. 19–32, May 2021, doi: 10.23919/JCC.2021.05.002.

[80] "Guidelines for the evaluation of radio interface technologies for IMT-2020," ITU, Geneva, Switzerland, ITU-Recommandation M.2412-0, 2017. [Online]. Available: https://www.itu.int/dms_pub/itu-r/opb/rep/R-REP-M.2412-2017-PDF-E.pdf

[81] L. Mohjazi, M. Al-Qutayri, H. Barada, K. Poon, and R. Shubair, "Deployment challenges of femtocells in future indoor wireless networks," in *Proc. IEEE GCC Conf. Exhibit. (GCC)*, Dubai, UAE, 2011, pp. 405–408.

[82] R. K. Saha, "Exploiting in-building small cell architecture for realizing dynamic spectrum sharing techniques," in *Proc. IEEE Int. Symp. Dyn. Spectr. Access Netw. (DySPAN)*, Newark, NJ, USA, 2019, pp. 1–2, doi: 10.1109/DySPAN.2019.8935772.

[83] M. Sasaki et al., "Path loss characteristics between different floors from 0.8 to 37 GHzin indoor office environments," in *Proc. Int. Symp. Antennas Propagat. (ISAP)*, Okinawa, Japan, 2016, pp. 66–67.

[84] Z. Zhang, Y. Xiao, Z. Ma, M. Xiao, Z. Ding, and X. Lei, "6G wireless networks: vision, requirements, architecture, and key technologies," *IEEE Veh. Technol. Mag.*, vol. 14, no. 3, pp. 28–41, Sep. 2019.

[85] S. Chen, Y.-C. Liang, S. Sun, S. Kang, W. Cheng, and M. Peng, "Vision, requirements, and technology trend of 6G: How to tackle the challenges of system coverage, capacity, user data-rate and movement speed," *IEEE Wireless Commun.*, vol. 27, no. 2, pp. 218–228, Apr. 2020, doi: 10.1109/MWC.001.1900333.

[86] C.-X. Wang, F. Haider, X. Gao, X.-H. You, Y. Yang, and D. Yuan, "Cellular architecture and key technologies for 5G wireless communication networks," *IEEE Commun. Mag.*, vol. 52, no. 2, pp. 122–130, Feb. 2014.

[87] G. Auer, V. Giannini, C. Desset, I. Godor, P. Skillermark, and M. Olsson, "How much energy is needed to run a wireless network?" *IEEE Wireless Commun.*, vol. 18, no. 5, pp. 40–49, Oct. 2011.

RONY K. SAHA received the B.Sc. degree in electrical and electronic engineering (securing second place in the batch) from the Khulna University of Engineering and Technology, Bangladesh, in 2004, the M.Eng. degree in information and communications technologies from the Asian Institute of Technology, Thailand, in 2011, and the Ph.D. degree in electrical engineering from Chulalongkorn University, Thailand, in 2017.

He is an Associate Professor with the Department of Electrical and Electronic Engineering, BRAC University, Dhaka, Bangladesh. He is a member of the Dynamic Spectrum Management Group, STAR Laboratory, Stanford University, CA, USA. He worked as a Visiting Professor of Electrical Engineering with Stanford University, Stanford, CA, USA, from February 2023 to May 2023. Further, he worked as a Postdoctoral Researcher with numerous laboratories, including the Optical Access Network Laboratory, Wireless Platform Laboratory, and Radio and Spectrum Laboratory, KDDI Research, Inc., Japan, from June 2017 to January 2022. Before that, he worked as a Lecturer and was later promoted to an Assistant Professor with American International University-Bangladesh, Bangladesh, from January 2005 to August 2013. From September 2013 to July 2014, he was with East West University, Bangladesh. He also worked as an LTE Research Intern with NOKIA Siemens Networks, Thailand, from December 2010 to January 2011. He has research experience in mobile wireless communications in universities and industries for about 15 years. He has authored 75 peer-reviewed, reputed, and recognized international journal and conference papers. He also filed an international patent. His current research interests include 5G and beyond ultra-dense HetNets, licensed and unlicensed spectrum sharing, policy, and management in multiple communication systems, and millimeter-wave communications.

Dr. Saha received the Highest Evaluation Score (Postdoctoral Fellow) with KDDI Research, Inc., for four consecutive fiscal half years from 2019 to 2020. He also received several Best Paper Awards at international conferences in Europe (including IARIA ICSNC 2020 in Portugal, ICWMC 2021 in France, and ICN 2021 in Portugal). Further, he has made several scientific contributions to the IARIA Conferences and received several Best Paper Awards (including ICSNC 2020 in Portugal, ICWMC 2021 in France, ICN 2021 in Portugal, and ICSNC 2021 in Spain). In recognition of outstanding scientific research results endorsed by international peers, exceptional scientific contribution to the IARIA events, and continuous leadership roles in IARIA conferences, he was awarded IARIA Fellow in the 2021 Fall/2022 Winter. He has been serving as an Associate Editor for the *Engineering*, Thailand, since 2019. He also served as a Reviewer for several recognized journals, including IEEE TRANSACTIONS ON SYSTEMS, MAN, AND CYBERNETICS: SYSTEMS, IEEE TRANSACTIONS ON COGNITIVE COMMUNICATIONS AND NETWORKING, IEEE OPEN JOURNAL OF ANTENNAS AND PROPAGATIONS, *IEEE Vehicular Technology Magazine*, IEEE TRANSACTIONS ON WIRELESS COMMUNICATIONS, IEEE TRANSACTIONS ON VEHICULAR TECHNOLOGY, IEEE WIRELESS COMMUNICATIONS, IEEE ACCESS, *Physical Communication* (Elsevier), *International Journal of Communication Systems* (Wiley), *Sensors* (MDPI), *Symmetry* (MDPI), *Mobile Information Systems* (Hindawi), and *Sustainability* (MDPI). He has been supporting several International Academy, Research, and Industry Association conferences either as a member of the technical program committee, a panelist, a steering committee member, or a tutorial speaker. He also served as a Steering Committee Member of IARIA ICSNC 2021. Previously, he served as a member of the Fronthaul Working Group, xRAN Forum, USA, and a TPC Member of the 2018 IEEE Global Communications Conference Workshops. He also served as the Session Chair for two sessions, namely, Radio Resource Management and Aerial Networks at the 2019 IEEE VTCFall, Honolulu, HI, USA, and the 2019 IEEE International Symposium on Dynamic Spectrum Access Networks Newark, Newark, NJ, USA, for the session Spectrum Sharing in 5G.